THE JOURNAL OF BIOLOGICAL CHEMISTRY VOL. 291, NO. 3, pp. 1348–1367, January 15, 2016

Transcriptional and Translational Modulation of *myo*-Inositol Oxygenase (Miox) by Fatty Acids

IMPLICATIONS IN RENAL TUBULAR INJURY INDUCED IN OBESITY AND DIABETES[*]

Received for publication, October 13, 2015, and in revised form, November 12, 2105 Published, JBC Papers in Press, November 17, 2015, DOI 10.1074/jbc.M115.698191

Tatsuya Tominaga[‡], Rajesh K. Dutta[‡], Darukeshwara Joladarashi[‡], Toshio Doi[§], Janardan K. Reddy[‡], and Yashpal S. Kanwar[‡1]

From the [‡]Department of Pathology, Feinberg School of Medicine, Northwestern University, Chicago, Illinois 60611 and the [§]Department of Nephrology, University of Tokushima, Tokushima, Japan

The kidney is one of the target organs for various metabolic diseases, including diabetes, metabolic syndrome, and obesity. Most of the metabolic studies underscore glomerular pathobiology, although the tubulo-interstitial compartment has been underemphasized. This study highlights mechanisms concerning the pathobiology of tubular injury in the context of *myo*-inositol oxygenase (Miox), a tubular enzyme. The kidneys of mice fed a high fat diet (HFD) had increased Miox expression and activity, and the latter was related to phosphorylation of serine/threonine residues. Also, expression of sterol regulatory element-binding protein1 (Srebp1) and markers of cellular/nuclear damage was increased along with accentuated apoptosis and loss of tubular brush border. Similar results were observed in cells treated with palmitate/BSA. Multiple sterol-response elements and E-box motifs were found in the *miox* promoter, and its activity was modulated by palmitate/BSA. Electrophoretic mobility and ChIP assays confirmed binding of Srebp to consensus sequences of the *miox* promoter. Exposure of palmitate/BSA-treated cells to rapamycin normalized Miox expression and prevented Srebp1 nuclear translocation. In addition, rapamycin treatment reduced p53 expression and apoptosis. Like rapamycin, *srebp* siRNA reduced Miox expression. Increased expression of Miox was associated with the generation of reactive oxygen species (ROS) in kidney tubules of mice fed an HFD and cell exposed to palmitate/BSA. Both *miox* and *srebp1* siRNAs reduced generation of ROS. Collectively, these findings suggest that HFD or fatty acids modulate transcriptional, translational, and post-translational regulation of Miox expression/activity and underscore Miox being a novel target of the transcription factor Srebp1. Conceivably, activation of the mTORC1/Srebp1/Miox pathway leads to the generation of ROS culminating into tubulo-interstitial injury in states of obesity.

Various metabolic diseases, including diabetes, obesity, and metabolic syndrome, adversely affect different compartments of the kidney to a varying degree culminating in chronic kidney disease and renal failure (1–4). For instance, in diabetic nephropathy (DN)[2] all the renal compartments, *i.e.* glomeruli, tubules, interstitium, and vasculature, are affected; however, the most notable lesions are confined to the glomerular compartment (5). Typical glomerular lesions of advanced DN are characterized by formation of Kimmelstiel-Wilson mesangial nodules (5). Like DN, obesity also affects the glomerular compartment, and the advanced pathologic lesions seen often are reminiscent of focal segmental glomerulosclerosis (1, 6). The shared pathogenetic events between DN and obesity that lead to renal glomerular damage include glomerular hyperfiltration, albuminuria, or proteinuria and oxidant stress in the form of increased expression of NADPH oxidase 4 (Nox4), although up-regulation of Nox4 may be related to decreased fatty acid oxidation in obesity (1, 5, 6). Interestingly, oxidant stress is regarded as the common denominator of various metabolic disturbances that perturb several signaling pathways and lead to renal damage in DN, and this situation is further complicated by activation of the renin-angiotensin system (1, 2, 5). In the obesity state, there is stimulation of the sympathetic nervous system that may very well also activate the renin-angiotensin system along with increased insulin resistance and hyperinsulinemia (1, 2). In addition to insulin resistance and hyperinsulinemia, aberrant levels of various adipokines, including those of leptin and adiponectin, have been observed, which apparently are directly related to the pathobiologic effects of fatty acids (7, 8). Fatty acid disturbances leading to obesity are well exemplified in various animal models, *i.e. ob/ob* and *db/db* mice with the defective leptin gene or its receptor, respectively (9, 10). One of the long term effects of obesity with co-existence of high fasting glucose includes development of metabolic syndrome, which is characterized by elevated lipid levels, low high density lipoproteins, hypertension, and associated insulin resistance (11).

[*] This work was supported by National Institutes of Health Grant DK60636 and the Manpei Suzuki Diabetes Foundation. The authors declare that they have no conflicts of interest with the contents of this article. The content is solely the responsibility of the authors and does not necessarily represent the official views of the National Institutes of Health.

[1] To whom correspondence should be addressed: Dept. of Pathology, Northwestern University Medical School, 300 E. Chicago Ave., Chicago, IL 60611. Tel.: 312-503-0004; Fax: 312-503-0627; E-mail: y-kanwar@northwestern.edu.

[2] The abbreviations used are: DN, diabetic nephropathy; Miox, *myo*-inositol oxygenase; HFD, high fat diet; Srebp, sterol regulatory element-binding protein; SRE, sterol-response element; CM-H_2DCF-DA, 5-(and-6)-chloromethyl-2′,7′-dichlorodihydrofluorescein diacetate, acetyl ester; DHE, dihydroethidium; SA-β-Gal, senescence-associated β-galactosidase; λ-PPase, λ protein phosphatase; pSrebp1, precursor form of pre-Srebp1; mSrebp1, mature form of Srebp1; IHC, immunohistochemical; MFI, mean fluorescence intensity; TPA, 12-*O*-tetradecanoyl phorbol-13-acetate; DCF, dichlorofluorescein; DCF-DA, DCF-diacetate.

Besides damage to the glomerular compartment by oxidant stress in various metabolic disturbances, peroxynitrite, generated by interaction of superoxide and nitric oxide, can also cause oxidant damage to the proximal tubule, which conceivably leads to tubulo-interstitial injury (5, 12, 13). On a long term basis, tubulo-interstitial injury could be reflected by mitochondrial dysfunctions and increased expression of extracellular matrix proteins; the changes are similar to those seen in the glomerular compartment. In line with the observations that there is hyperlipidemia and high levels of non-esterified fatty acids in type 2 diabetes, Zhang *et al.* (14) reported that a high fat diet induces glomerular as well as tubulo-interstitial damage in *db/db* mice, which could be alleviated by the inhibition of hsp90 accompanied with reduced levels of renal nitrotyrosine and mitochondrial Ca^{2+} efflux. These observations suggest that various metabolic disturbances, whether related to hyperlipidemia or hyperglycemia, induce tubular damage and subsequent tubulo-interstitial injury, although this concept has been sparsely described in the literature. In support of this concept, recent investigations suggest that excessive leakage of albumin during glomerular proteinuria in various metabolic disturbances may not necessarily be the culprit in the induction of tubulo-interstitial injury; rather it is due to the fatty acids bound to albumin (15–17). Albumin filtered across renal glomerulus is known to be largely reabsorbed by proximal tubules by receptor-mediated endocytosis, thus suggesting that this segment of the nephron would be readily vulnerable to fatty acid-induced injury (18). Albumin can bind efficiently to fatty acids and transport the fatty acids to the tubules, and thus it is conceivable that fatty acid-bound albumin can induce tubulo-interstitial injury. In this regard, the *in vitro* studies by Ruggiero *et al.* (19) suggest that exposure of tubular cells to palmitate bound to albumin, but not albumin itself, induces mitochondrial dysfunctions, redox imbalance, and deactivates antioxidant protein peroxiredoxin 2, ultimately leading to peroxide-mediated cellular apoptosis. Overall, the above discussion emphasizes the importance of the tubulo-interstitial compartment in bearing the brunt of injury in various metabolic disorders, such as diabetes and obesity.

Several years ago we reported the discovery of one of the metabolic enzymes, *i.e. myo*-inositol oxygenase (Miox), that is exclusively expressed in the renal proximal tubular compartment and is up-regulated in the diabetic state (20). The enzyme metabolizes *myo*-inositol to glucuronic acid via the glucuronate-xylulose pathway, and its metabolites enter into the pentose pathway (21). The enzyme activity of Miox is dependent upon phosphorylation of its serine/threonine residues (22). The *miox* promoter includes osmotic, carbohydrate, and both oxidant- and antioxidant-response elements, and its transcription is heavily influenced by organic osmolytes, high glucose ambience, and oxidant stress (22–24). Further initial examination of the *miox* promoter suggested that it also includes multiple sterol-response elements (SRE) and E-box motifs, which led us to investigate its transcriptional and translational modulation by fatty acids and in states of obesity.

Experimental Procedures

Reagents—HK-2 and LLC-PK1 cells (renal proximal tubular cell lines) were purchased from the American Type Culture Collection (ATCC). TRIzol and pcDNA3.1 plasmid vector were obtained from Invitrogen. Other reagents were purchased from the following vendors: Dulbecco's modified Eagle's medium (DMEM), M199 media, fatty acid-free BSA (A7030), sodium palmitate (P9767), insulin, and anti-β-actin antibody from Sigma; OptiMEM I reduced serum medium, fetal bovine serum (FBS), antibiotic-antimycotic, Fast SYBR Green Master Mix, and TO-PRO®-3 iodide from Life Technologies Inc.; high fat diet chow (HFD) (5.24 kcal/g, 60% fat, 20% protein, 20% carbohydrate, D12492) from Research Diet Inc.; anti-Srebp1, anti-Bax, anti-p53, anti-Bcl2, and anti-His probe antibodies from Santa Cruz Biotechnology; protein G-agarose and insulin ELISA kit from Millipore; *srebp1* siRNA and *miox* siRNA from OriGene Technologies; LightShift Chemiluminescent EMSA kit and Infinity cholesterol reagent from Thermo Scientific; QuikChange multisite-directed mutagenesis kit from Stratagene; pGL4 promoter vector, pRL-CMV-*Renilla*, FuGENE 6, and Dual-Luciferase® kit from Promega; rapamycin from LC Laboratories; Accu-Chek glucometer from Roche Applied Science; anti-pH2AX antibody from Cell Signaling Technologies; anti-phospho serine/threonine-specific PKA substrate antibody, anti-phosphoserine-specific PKC substrate antibody, anti-phosphothreonine antibody, and anti-phosphotyrosine antibody from Cell Signaling Technologies.

Animal Studies—Eight week old male CD1 mice and rats were purchased from Harlan Co. (Indianapolis, IN) and housed in institutional animal facilities. Before initiating the experiments the animals were acclimatized for 1 week in rooms with a 12-h light/dark cycle at a temperature of 22 °C with 50% humidity. The mice and rats had free access to food and water. The control animals received a normal mouse/rat pelleted chow. The experimental animals received a high fat diet in the form of chow pellets and were sacrificed at 2, 4, and 6 weeks. Likewise, in another set of experiments, mice receiving control or HFD were concomitantly treated with rapamycin (4 mg/kg, i.p., daily). After 6 weeks, the serum insulin levels were measured using commercial rat/mouse insulin ELISA kits (Millipore). Serum cholesterol was measured by using Infinity cholesterol reagent (Thermo Scientific). Blood glucose levels were measured by Accu-Chek meter (Roche Applied Science). Prior to sacrifice, 24-h urine collections were made for determination of protein excretion by SDS-PAGE. All animal studies were approved by the Animal Care and Use Committee of Northwestern University, and Tokushima University, Japan.

Morphology Studies—Three-μm-thick sections were prepared from paraffin-embedded tissues and subjected to periodic acid-Schiff staining. For immunohistochemistry to detect the expression of various proteins, the avidin-biotin complex method was employed (20, 22, 24). The tissue sections were de-paraffinized, rehydrated with PBS, and treated with 0.3% H_2O_2. Then the tissue sections were subjected to an antigen retrieval procedure in the HistoVT One by following the vendor's instructions (Nacalai Tesque, Inc., Japan). After blocking with 5% normal goat serum in PBS, the sections were incu-

bated with various primary antibodies. Miox expression in the kidneys was gauged by immunofluorescence microscopy, as described previously (20, 22, 24). Briefly, 4-μm-thick cryostat sections were prepared, air-dried for an hour, and fixed with 4% para-formaldehyde for 10 min at 22 °C. After equilibrating the sections with PBS, they were incubated with the polyclonal Miox antibody at 37 °C for 1 h, washed with PBS, and re-incubated with goat anti-rabbit IgG antibody conjugated with FITC (Sigma) for another hour. Following a PBS wash, the tissue sections were covered with a drop of buffered glycerol, coverslip-mounted, and examined using a Zeiss microscope equipped with UV epi-illumination (Carl Zeiss MicroImaging, Inc., Thornwood, NY).

Other morphologic studies included the assessment of apoptosis in kidney tissues or HK-2 cells by using the TUNEL method (25). De-paraffinized sections or frozen cryostat sections of the kidneys were digested with proteinase K (240 unit/ml, Promega, Madison, WI) for 30 min at 22 °C. After a rinse with PBS, the sections were incubated with TUNEL reagents (Roche Applied Science). The cells were processed for evaluation of apoptosis as follows. The HK-2 cells were fixed with 4% fresh paraformaldehyde for 20 min at 22 °C. They were permeabilized with 0.1% Triton X-100 at 4 °C for 1 min and then incubated with TUNEL reagents at 37 °C for 1 h, as per instructions from the vendor. The nuclei were also stained with TO-PRO-3®-iodide. The cells undergoing apoptosis were identified as fluorescent nuclei with a UV microscope.

For senescence-associated β-galactosidase (SA-β-gal) staining, 4-μm-thick cryostat kidney sections were prepared from freshly frozen kidneys (26). The sections were immersed in a 0.2% glutaraldehyde fixative solution containing 0.1 M phosphate buffer, pH 7.2, 5 mM EGTA, 2 mM $MgCl_2$, and 0.1% Nonidet P-40 for 20 min. Sections were washed with PBS and then immersed in SA-β-Gal staining solution (0.1 M phosphate buffer, pH 7.2, 2 mM $MgCl_2$, 0.01% sodium deoxycholate, 0.02% Nonidet P-40, 5 mM potassium ferricyanide, 5 mM potassium ferrocyanide, 20 mM Tris-HCl, pH 7.3, and 1 mg/ml X-gal). Sections were incubated in the dark at 37 °C for 16–18 h. They were then washed with PBS and counterstained for 5 min with 0.1% nuclear fast red.

Preparation of Fatty Acid Conjugates with Bovine Serum Albumin (BSA)—A preparation of palmitate-conjugated BSA was made by modifying a previously described method (27). A working solution of 5 mM palmitate/BSA was prepared by conjugating BSA with palmitate as follows. One g of Ultra Fatty Acid-free BSA was mixed with 20 ml of 0.15 M NaCl in a small beaker. This beaker was placed in a larger 1-liter beaker with pre-warmed water, and the temperature was maintained at 37 °C while being stirred on a hot plate. The dissolved BSA was filtered through a 0.45-μm filter, and the pH was adjusted to pH 7.4. The filtered BSA was constantly stirred at 37 °C as indicated above. In another beaker, 279 mg of sodium palmitate was mixed with 10 ml of 0.15 M NaCl. The palmitate solution was placed in a 70 °C water bath with frequent gentle shaking until completely dissolved. Then 0.5 ml of the heated palmitate solution was added to 9.5 ml of BSA solution while stirring at 37 °C for 1 h. The dissolved palmitate-conjugated BSA was re-filtered through a 0.45-μm filter and used.

Cell Culture Studies—HK-2 cells were grown in low glucose DMEM supplemented with 5% heat-inactivated FBS, 100 units/ml penicillin, and 100 μg/ml streptomycin. LLC-PK1 cells were grown in low glucose M199 medium supplemented with 3% heat-inactivated FBS, 100 units/ml penicillin, and 100 μg/ml streptomycin. The cells were maintained in a humidified atmosphere of 5% CO_2, 95% air at 37 °C. Approximately 2.2×10^6 cells were seeded on 55-cm^2 culture dishes and maintained to achieve 80% confluency. The cells were then treated with various concentrations of palmitate/BSA (10–300 μM) for 24–48 h. For the inhibition assay, cells were treated with palmitate/BSA in the presence/absence of rapamycin (10 mM), *srebp1* siRNA, and *miox* siRNA.

Enzymatic Activity of Miox in Kidneys and LLCPK-1 Cells—Miox activity was determined, as described previously (24). Briefly, kidney cortices of mice receiving normal and high fat diet or cells undergoing various treatments were homogenized in a sodium acetate or phosphatase buffer. The protein concentration of the homogenate was adjusted to 100 μg/ml, and 50 μl of homogenate was used from each variable for determining the Miox activity. The reaction was carried out at 30 °C for 30 min in a volume of 500 μl containing 50 mM sodium acetate, 1 mM ferrous ammonium sulfate, 2 mM L-cysteine, and 60 mM *myo*-inositol. The reaction was terminated by boiling followed by precipitation with 3% TCA. Following centrifugation at $1,000 \times g$ for 5 min, the D-glucuronate concentration was determined in the supernatant with the addition of double the volume of freshly prepared orcinol reagent (40 mg of orcinol and 9 mg of $FeCl_36H_2O$ dissolved in 10 ml of concentrated HCl) (28). Spectrometric readings were made at $A_{660\,nm}$. Miox activity was averaged from four different experiments or animals per variable. For phosphatase treatment, the kidney homogenates or cellular lysates from various experimental variables were prepared and treated with protein λ-phosphatase (λ-PPase; New England Biolabs) for 1 h at 30 °C. The phosphatase reaction was carried out in a mixture containing 50 mM Tris-HCl, pH 7.8, 5 mM DTT, 2 mM $MnCl_2$, 100 μg/ml BSA, 100 units of λ-PPase, and 50 μl of homogenate protein solution in a total volume of 500 μl, following which the samples were processed for determination of Miox activity. In another set of experiments, the effect of various kinase activators and inhibitors on the potentiation or dampening of the Miox activity was carried out following 24 h of palmitate/BSA treatment. Various activators and inhibitors used were as follows: PKA activator forskolin (0.2 μM) and inhibitor H89 (0.2 μM); phosphoinositide-dependent protein kinase-1 (PDK1)/PI3K inhibitor wortmannin (0.5 μM) and activator insulin (100 nM); PKC activator 12-*O*-tetradecanoyl phorbol-13-acetate (TPA, 0.2 μM) and inhibitor calphostin (0.05 μM).

Immunoblot Analyses—Cytoplasmic and nuclear extracts were prepared from HK-2 or LLCCK-1 cells, as detailed previously (22). Protein concentrations in the extracts were measured by the Bradford method, and equal amounts of protein were loaded in each lane of the gels subjected to SDS-PAGE and blotted onto nitrocellulose membrane. Membranes were incubated with 1 mg/ml diluted from each of the primary antibodies for 15 h at 4 °C in Tris-buffered saline + Tween 20 (TBS-T) supplemented with 5% nonfat dried milk. After a brief wash

with TBST, the membranes were then incubated with 1:4,000 diluted goat anti-rabbit IgG (Santa Cruz Biotechnology) or 1:10,000 diluted goat anti-mouse IgG (Sigma) as secondary antibodies conjugated with horseradish peroxidase (HRP). Autoradiograms were prepared using the enhanced chemiluminescence (ECL) detection system (Thermo Scientific). Equal loading of the samples was confirmed by probing the immunoblots with mouse β-actin or laminB1 antibodies at a dilution of 1:10,000.

Immunoprecipitation and Western Blot Analyses with Phosphoamino Acid-specific Antibodies—To assess whether the high activity of Miox by HFD administration and palmitate/BSA treatment was due to phosphorylation of a given specific amino acid residue by different kinases, the treated cells and kidney homogenates were lysed in a radioimmune precipitation assay buffer containing protease and phosphatase inhibitors, as described previously (22, 24). Equal amounts (50 μg of protein) of the cell lysates/kidney homogenates were used for immunoprecipitation with the following antibodies: anti-phosphoserine/threonine-specific PKA substrate antibody, anti-phosphoserine-specific PKC substrate antibody, anti-phosphothreonine antibody, and anti-phosphotyrosine antibody (Cell Signaling Technology). The immunoprecipitates were subjected to 10% SDS-PAGE. The proteins were then transferred onto PVDF membranes, and the blots were prepared. They were then probed with polyclonal anti-Miox antibody.

Isolation of miox Transcripts and Generation of Reporter Constructs—A DNA fragment was isolated from the human genomic DNA (Promega) and used as a template for generation of PCR products spanning the *miox* promoter region by employing a common antisense primer 5′-GTACCCCAGACCCATGAGTGGTGGCAGTGGAAGTA-3′ and the following sense primers: 5′-GGGGGTAC(C/G)TCCCACCTCCTAACCTATC-3′ (−1499 to +30), 5′-GGGGGTAC(C/T)GTGGCCGAACTCTAGGC-3′ (−828 to +30), and 5′-GGGGGTAC(C/C)AAGTGGGAGGCTGG-3′ (−261 to +30). The DNA fragments were cloned into pGL4.16 promoter vector (Promega). A KpnI site, GGTACC (underlined), was included in the primers. The inserts were sequenced and their orientation confirmed by using vector-specific primer 5′-CTAGCAAAATAGGCTGTCCC-3′. The upstream 5′ sequence of human *miox* and its homologues were retrieved from NCBI. Transcription-factor-binding motifs and promoter predication were searched on line. For creating pGL4 mutation constructs, the pGL4 (−1499 to +30) construct vector was modified using QuikChange multisite-directed mutagenesis kit per manufacturer's instructions. Mutagenic primer 5′-GATACAGCCTTGACCCCCAGG**T**GCTGACATTCTAGGGGGAGA-3′ (mutated SRE site is in underlined) was used to mutate the SRE site (GACCCCCAGG**G**GCTGACATT) in the pGL4 inclusive of the *miox* promoter (−1499 to +30). The mutation in the modified construct was confirmed by nucleotide sequencing.

Transfection of Cells and Luciferase Assays—The reporter plasmid constructs (pGL4 −1499 to +30, −828 to +30, and −261 to +30) were transfected into exponentially growing HK-2 cells (1×10^5 cells) seeded onto 24-well culture plates in Opti-MEM I medium and allowed to grow for 12 h. The transfection was carried out by using 1.5 μl of FuGENE 6 and 1 μg of reporter plasmid constructs. Luciferase activity was normalized to *Renilla* luciferase activity following co-transfection with pRL-CMV-*Renilla* (100 ng), which served as the optimized equalization control. Assays for both firefly and *Renilla* luciferase activity were carried out 24 h post-transfection using a commercial Dual-Luciferase® kit and a TD 20/20 luminometer according to the instructions provided by the manufacturer. Basal promoter activity was determined in cells transfected with reporter construct pGL4.16 only. For comparison between fatty acid-free BSA and palmitate/BSA, 24 h post-transfection of the reporter plasmid-nonliposomal complex, the culture medium was replaced with Opti-MEM I containing 100 μM BSA or palmitate/BSA.

Electrophoretic Mobility Shift Assays (EMSA)—Nuclear extracts were prepared from HK-2 cells, as described previously (22). EMSA were performed using a Thermo Fisher LightShift chemiluminescent EMSA kit per instructions provided by the manufacturer. Briefly, single-stranded oligomers were custom-synthesized by Integrated DNA Technologies. Their sequences were as follows: −1048 to −1017, 5′-GCACCCCACTGCCCTCTCTCCTGCCCCAGCCG-3′, which corresponded to nucleotide stretches spanning human SRE. Both sense and complementary oligomers were labeled using a biotin 3′-end DNA labeling kit and by following the manufacturer's instructions. For EMSA, the binding reactions were carried out using 10 μg of nuclear protein and 20 fmol of biotin end-labeled DNA in a 20-μl volume containing 2.5% glycerol, 5 mM $MgCl_2$, 50 ng/μl poly(dI·dC), and 0.05% Nonidet P-40. The reaction mixtures were incubated at 22 °C for 30 min. The samples were then loaded onto 4% polyacrylamide non-denaturing minigels, and electrophoresis was carried out in a 0.5× running TBE buffer. DNA-protein complexes in the gels were then transferred onto a Hybond-N^+ membrane by wet transfer in 0.5× TBE buffer and immobilized by UV cross-linking. For specificity, the blots were probed with Srebp1 antibody. The biotin-labeled reaction products were visualized by treating the blots with streptavidin horseradish peroxidase conjugate followed by incubation with ECL chemiluminescent reagents.

Chromatin Immunoprecipitation (ChIP) Assays—ChIP assays were also carried out to assess the binding of Srebp1 to the promoter region of human *miox*. The HK-2 cells were cultured in 100-mm Petri dishes and treated with 10–100 μM palmitate/BSA for 24 h. The ChIP assay was performed, as described previously (22). Cross-linking of DNA and protein was carried out by addition of 1% formaldehyde into the cell medium and incubated for 15 min. The formaldehyde was quenched by the addition of 0.125 M glycine for 5 min. The cells were then washed with cold PBS, scraped from the dishes, and centrifuged at 500 × *g* for 5 min. The pellet was resuspended in 300 μl of swelling buffer (25 mM HEPES, pH 7.8, 1.5 mM $MgCl_2$, 10 mM KCl, 0.1% Nonidet P-40, 1 mM DTT, 0.5 mM PMSF) and incubated on ice for 10 min. The DNA fragmentation for preparation of oligonucleotides was achieved with the treatment of micrococcal nuclease for 20 min at 37 °C. The reaction was terminated by adding 10 μl of 0.5 M EDTA, pH 8.0. This was followed by a brief centrifugation at 10,000 × *g* for 3 min. The pellet was resuspended in 250 μl of sonication buffer (50 mM HEPES, pH 7.9, 140 mM NaCl, 1% Triton X-100, 0.1% sodium deoxycholate, 0.1% SDS, and 0.5 mM PMSF) and incubated on

ice for 10 min and then sonicated to generate 200–1,000-bp DNA fragments. The sonicated suspension was centrifuged at 15,000 × *g* for 15 min to remove the insoluble debris. The soluble chromatin was diluted to 1:10 with ChIP dilution buffer (16.7 mM Tris-HCl, pH 8.1, 167 mM NaCl, 1 mM EDTA, 1% Triton X-100, and 0.01% SDS). It was pre-cleaned by incubation with protein G-Sepharose for 2 h at 4 °C. The samples were then re-centrifuged, and an aliquot (800 μl) was saved as input DNA. The remainder was processed for immunoprecipitation with Srebp1 antibody followed by incubation with protein G-Sepharose beads. Samples with normal IgG were also used as a negative control. The Sepharose beads were centrifuged and washed twice, first with 1 ml of low salt washing solution (20 mM Tris-HCl, pH 8.1, 150 mM NaCl, 2 mM EDTA, 1% Triton X-100, and 0.1% SDS) and then with 1 ml of high salt washing solution (20 mM Tris-HCl, pH 8.1, 500 mM NaCl, 2 mM EDTA, 1% Triton X-100, and 0.1% SDS). The beads were then washed with a LiCl washing solution (10 mM Tris-HCl, pH 8.1, 1 mM EDTA, 1% deoxycholic acid, 1% Nonidet P-40, and 0.25 M LiCl) and then twice with 1 ml of Tris/EDTA buffer. DNA fragments from the samples were eluted by adding 400 μl of elution buffer (50 mM Tris-HCl, pH 8.0, 50 mM $NaHCO_3$, 1 mM EDTA, and 1% SDS) and then incubated at 65 °C for 10 min. After addition of 16 μl of 5 M NaCl, the samples were further incubated at 65 °C for 4 h for de-cross-linking. Similarly, samples of input DNA were de-cross-linked. One μl of DNase-free RNase A (10 mg/ml) was added and incubated at 37 °C for 30 min. This was followed by addition of 10 μl of proteinase K (2 mg/ml), and then the samples were incubated at 55 °C for 1 h. After a phenol/chloroform extraction and addition of 1 μl of glycogen (20 mg/ml), the DNA was precipitated with 40 μl of 3 M sodium acetate and 1 ml of ethanol. The precipitates of ChIP and input samples were resuspended in 20 μl of 10 mM Tris/EDTA buffer and used for PCR analyses. The primers used for ChIP-PCR included regions spanning SRE motifs included in the *miox* promoter from −1,499 to −1,229 bp. The primer sequences were 5′-GTCCCACCTCCTGAACCTATCCAG-3′ (sense) and 5′-TGACTTCCTGTGGCACTCAGCA-3′ (antisense), with an expected size of an amplified product of 271 bp.

Generation of Eukaryotic Expression Constructs and Stable Transfectants—An *srebp1* cDNA was generated by RT-PCR with *srebp1*-specific primers, and it was cloned into pcDNA3.1/V5-His TOPO vector (Invitrogen) and amplified in an *Escherichia coli* system, as described previously (29). For cloning of mouse cDNA, *srebp1* was amplified using the mouse kidney cDNA and the respective sense and antisense primers 5′-GCCACCATGGACGAGCTGGCCTTCG-3′ with Kozak sequence and 5′-GCCCCAGCCGAAAAGCGAG-3′. The plasmid constructs were then transfected into LLC-PK1 cells, and stable transfectants were selected by growing cells in the presence of G418.

RNA Extraction and Quantitative Real Time PCR—Total RNA was isolated from the kidney using TRIzol reagent (Invitrogen), and cDNA was synthesized using Go Script reverse transcription system (Promega). The mRNA level was quantified using Step One Plus System real time PCR (Applied Biosystems). A 20-μl total reaction mix included 100 ng of cDNA, 50 nmol/liter forward/reverse primers, and 1× Fast SYBR Green Master Mix (Life Technologies, Inc.). 18S rRNA was used as an internal control, and the amount of mRNA was calculated by the comparative C_T method. All the data were derived from quadruplicate PCRs. The levels of *miox*, *srebp1* mRNA, and 18S rRNA were determined. The primers used were as follows: *miox* forward, 5′-TGTCTTCACCACCTACAAGCTC-3′, and reverse, 5′-GGCCTCCATGACTGTCATTTTC-3′; and *srebp1* forward, 5′-AGTGACTTCCCTGGCCTATTTG-3′, and reverse, 5′-TCAAGAGAGGAGCTCAATGTGG-3′; and 18S rRNA forward, 5′-CGAGCCGCCTGGATACC-3′, and reverse, 5′-CAGTTCCGAAAACCAACAAAATAGA-3′.

Determination of Intracellular ROS—The status of cellular ROS was evaluated both by fluorescent microscopy and flow cytometry using 5-(and-6)-chloromethyl-2′,7′-dichlorodihydrofluorescein diacetate, acetyl ester (CM-H_2DCF-DA) dye. The dye following its diffusion into the cell gets deacetylated by cellular esterases and then oxidized by intracellular ROS into a highly fluorescent compound DCF, which can be detected by fluorescent microscopy or flow cytometry with excitation at 488 and emission at 520 nm. About 5 × 10^5 HK-2 cells were seeded (on coverslips for microscopy) in a 6-well plate and treated with various concentrations of palmitate/BSA (30–300 μM) for 24 h. In another set of experiments, the palmitate/BSA-treated cells were also subjected to *srebp1* or *miox* siRNA treatment for their respective gene disruption. Cells were then washed twice with PBS and each wash was 5 min. 5 mM stock of CM-H_2DCF-DA in DMSO was diluted in PBS to make a final concentration of 5 μM. Cells were then incubated with 5 μM CM-H_2DCF-DA probe for 15 min at 37 °C in the dark. They were re-washed three times with PBS, each wash was 5 min, and then processed for microscopic examination. For flow cytometry-based detection of ROS, cells were gently scraped off the plates with a rubber policeman and transferred into fluorescence-activated cell sorting tubes for staining. Cells were stained with 5 μM CM-H_2DCF-DA for 15 min at 37 °C in the dark. They were then washed twice with PBS and resuspended in 300 μl of PBS and processed for acquisition of fluorescence with a flow cytometer. Then mean fluorescent intensity of the CM-H_2DCF-DA was measured using standard operational procedures of flow cytometry and employing FACSDiva software (BD Biosciences).

MitoSOX Staining of Cells—Mitochondrial superoxide (O_2^-) generation was detected by using a specific mitochondrial superoxide indicator, MitoSOX Red (Molecular Probes). HK-2 cells were seeded in 6-well plates and treated with various concentrations of palmitate/BSA (30–300 μM) for 24 h, as described above. After transferring the cells into the FACS tubes, they were incubated with 5 μM MitoSOX for 15 min at 37 °C in the dark. Following two PBS washes, the cells were subjected to flow cytometric measurements, and mean fluorescence intensity was determined.

Determination of ROS in Kidney Tissues—For detection of ROS in kidney tissues, transverse renal slices were prepared from mice fed control and high fat diets. They were embedded in OCT compound in a plastic mold and immediately frozen in liquid nitrogen. The embedded tissues were mounted on metallic stubs. About 8 μm thick frozen sections of the kidney were

prepared using Leica cryostat and transferred onto glass slides. The tissue sections were then air-dried for 5 min at 22 °C. To remove OCT compound from tissues, the glass slides were rinsed twice with PBS. The sections were then incubated with 5 μM CM-H_2DCF-DA or 10 μM DHE for 15 min at 37 °C. They were washed with PBS twice for 5 min each. A drop of mounting media was placed onto the tissue sections. They were then covered with glass coverslips and examined with a fluorescence microscope equipped with UV epi-illumination.

Statistical Analyses—Results were expressed as mean ± S.D. following statistical analyses. Student's *t* test was used to compare the data between the two groups. A p value of <0.05 was considered to be statistically significant.

Results

The findings described in this section include the induction of Miox expression and activity in a hyperlipidemic state via phosphorylation of its potential PKC-, PKA-, and PDK1-phosphorylating sites and how HFD administration or exposure of fatty acids to renal tubular cells *in vitro* affects its translational and transcriptional activities. The latter seems to be largely influenced by unique DNA E-box overlapping sites for the binding of transcription factor Srebp localized in its promoter. Intriguingly, fatty acid-induced Miox up-regulation also led to a notable oxidant stress in renal tubular cells.

Effect of HFD and Albumin-bound Fatty Acids on Miox Expression and Activity—Administration of HFD to CD1 mice over a period of 2–6 weeks induced a tremendous increase in the expression of Miox, as assessed by immunofluorescence microscopy (Fig. 1, *A versus B*). The increased expression, highlighted by green fluorescence, was exclusively confined to the tubular compartment of the kidney cortex, although no expression was seen in the glomeruli (Fig. 1, *A* and *B*, *arrowheads*). Also, besides the increased expression in superficial cortical tubules, it also extended into the deeper cortex. The expression was time-dependent because it steadily increased over a period of 6 weeks, as assessed by immunoblot analyses, whereas β-actin expression was unchanged (Fig. 1*C*). Likewise, Miox activity was increased notably up to 4 weeks, although a mild increase was also seen at 6 weeks (Fig. 1*D*). This increase in the activity was reduced to normal levels with treatment of λ-PPase, suggesting that the increase in the activity was phosphorylation-dependent. These *in vivo* observations were confirmed by *in vitro* experiments where LLCPK-1 cells were exposed to various concentrations of palmitate-conjugated BSA. A dose-dependent increase in Miox expression and activity was observed at a concentration range of 10–300 μM of palmitate/BSA, although no change was observed with BSA treatment alone (Fig. 1, *E* and *F*). Similar to *in vivo* results, the λ-PPase treatment reduced Miox activity to basal levels in LLCPK-1 cells. During these *in vitro* experiments, a certain degree of apoptosis was observed in these cells, and thus in light of these observations apoptogenic Bax expression was assessed to rule out any cytotoxic effect. Concomitant with Miox up-regulation, a dose-dependent increased Bax protein expression was observed following palmitate/BSA treatment of LLCPK-1 cells (Fig. 1, *G–I*).

Effect of HFD and Albumin-bound Fatty Acids on the Phosphorylation of Miox and Its Activity—With respect to phosphorylation of Miox, the next question addressed was which amino acid residues are affected by HFD or palmitate/BSA treatment because one of our previous publications suggests that Miox is differentially phosphorylated in a diabetic state or under high glucose ambience. This was accomplished by using antibodies directed against various phosphorylated amino acid residues. Immunoprecipitation was performed on kidney homogenates or cellular lysates with substrate-specific phosphoantibodies to PKA (Ser/Thr) and PKC (Ser) and to phosphothreonine and phosphotyrosine residues. This was followed by Western blot analyses with anti-Miox antibody using equal concentrations of proteins in immunoprecipitated samples. A time-dependent (2–6 weeks) increased phosphorylation was observed following HFD administration in kidney samples where immunoprecipitation was carried out with phosphoantibodies directed against serine and threonine residues (Fig. 2*A*). No increase was observed in samples immunoprecipitated with anti-phosphotyrosine antibody. Similarly, a dose-dependent increase in phosphorylation at serine and threonine residues was observed in cells treated with various concentrations of palmitate/BSA (Fig. 2*B*). No increase in phosphorylation of tyrosine residues was observed, suggesting that these residues in Miox are unaffected by phosphorylation following HFD administration or palmitate/BSA treatment. The latter treatment also led to an increase in Miox activity in LLCPK-1 cells. Concomitant treatment with palmitate/BSA and activators of PKA (forskolin), PDK/PI3K (insulin), and PKC (TPA) further increased Miox activity (Fig. 2*C*). Although concomitant treatment with respective inhibitors, *i.e.* H89 (PKA), wortmannin (PI3K), and calphostin (PKC), reduced the activity below the levels induced by palmitate/BSA alone, this confirmed that fatty acid-induced activity is phosphorylation-dependent (Fig. 2*C*). Because fatty acids seem to modulate expression of Miox, we proceeded to investigate the status of proteins that regulate fatty acid and cholesterol biosynthesis. We focused on Srebp1 in the context of Miox pathobiology.

Effect of Hyperlipidemia, Palmitate/BSA, and Insulin on Miox and Srebp1 Expression—Treatment of HK-2 cells with palmitate/BSA (100 μM) for 24 h induced an increased Miox expression with a concomitant decrease in the membrane-bound precursor form of pre-Srebp1 (pSrebp1, 120 kDa) in the cytoplasmic fraction. Simultaneously, with its recruitment and cleavage, the mature form (mSrebp1, 68 kDa) translocated into the nucleus, as assessed by immunoblot analyses (Fig. 3*A*). No change in the expression of β-actin or laminB1 was observed. The dissociation of mSrebp from Golgi saccules following cleavage with an increase and decrease in the nuclear and cytoplasmic expression, respectively, was quantified and included as bar graphs (Fig. 3, *B* and *C*). Srebp1 is believed to serve as a link in changes in insulin levels and expression of genes that modulate systemic energy metabolism, *e.g.* fatty-acid synthase and leptin (30). Thus, it is activated during nutritional abundance and adiposity and is associated with excessive secretion of insulin in early phases of obesity, a vital component of metabolic syndrome with increased insulin and glucose levels and a certain degree of insulin resistance (30–32). Because Miox is

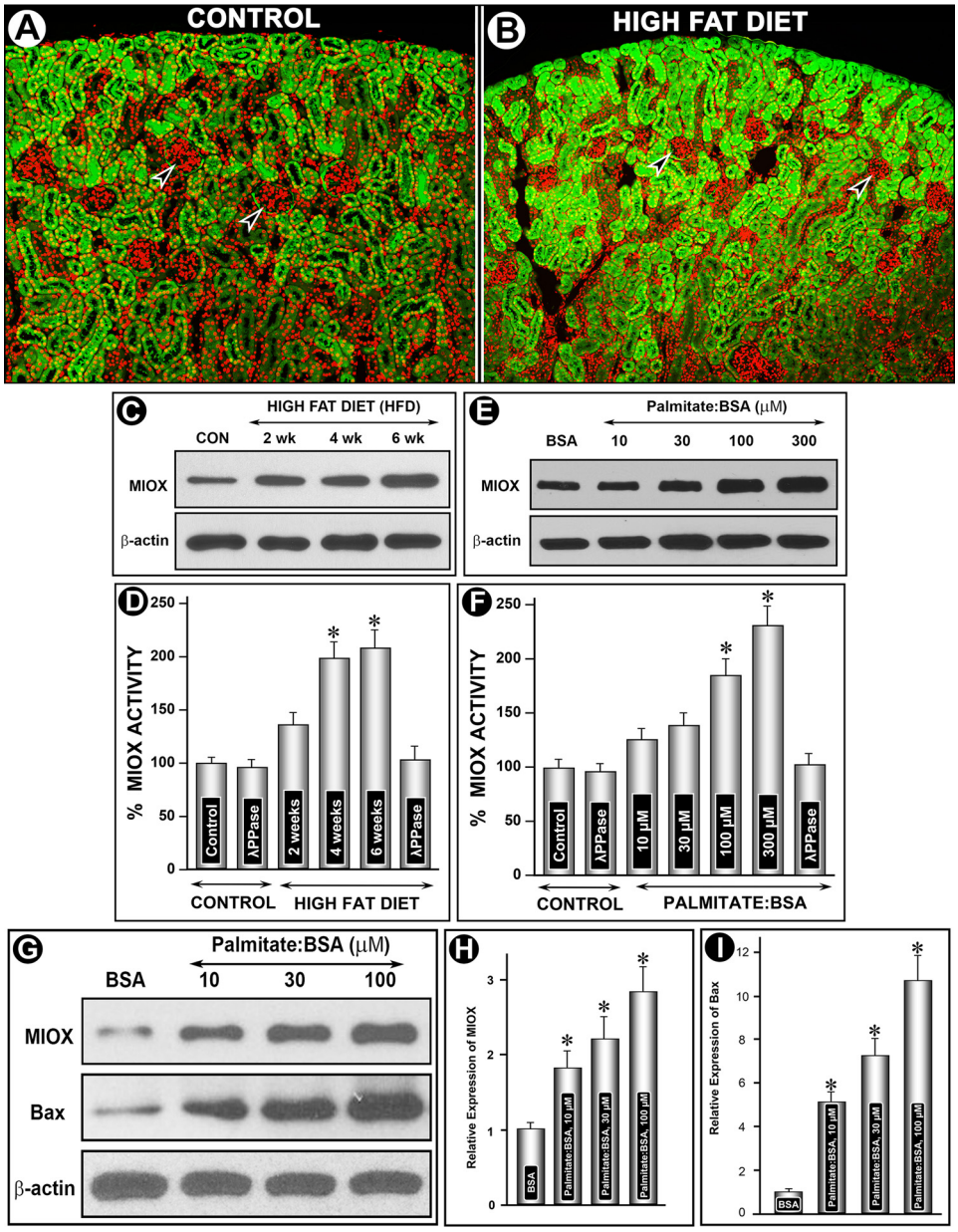

FIGURE 1. **Modulation of Miox expression and activity and of Bax by HFD and albumin-bound fatty acids.** Following HFD administration an increased expression of Miox was seen in kidney cortical tubules (*green fluorescence*, *A* and *B*), although no expression was seen in glomeruli (*arrowheads*). Miox expression extended into deeper cortex in mice fed an HFD diet (*B*). By immunoblot analyses, the expression seemed to be time-dependent, and it increased over a period of 6 weeks, whereas the β-actin expression was unchanged (*C*). A concomitant time-dependent increase in Miox activity was also observed, which was normalized following λ-PPase treatment, suggesting that the activity was phosphorylation-dependent (*D*). *In vitro,* a dose-dependent increase in the expression and activity of Miox was also observed in cells treated with palmitate/BSA (*E* and *F*). Similarly, a dose-dependent increase in the BAX's expression was observed with the palmitate/BSA treatment, suggesting preserved cellular integrity at least within the concentration range used (*G–I*). *, $p < 0.01$ *versus* control, $n = 4$.

transcriptionally up-regulated by high glucose ambience, we evaluated whether insulin causes a concomitant increase in the expression of Miox and mSrebp1. A dose-dependent increase in the expression of Miox was observed following insulin (10–1,000 nM) treatment (Fig. 3, *D* and *F*). At the same time, a dose-dependent increase in the mSrebp1 was observed (Fig. 3, *E* and *G*), suggesting a temporal relationship between the up-regulation of Miox and translocation of mSrebp1. The *in vivo* results in mice or rats were similar to those seen in cultured cells exposed to palmitate/BSA. Like Miox, the HFD administration over a period of 6 weeks resulted in a marked time-dependent up-regulation of mSrebp1 (Fig. 3*H*). No change in the laminB1 expression was observed. These observations were further substantiated by immunohistochemical (IHC) studies performed on kidney sections of mice fed control and HFD diets, using anti-Srebp1 antibody (Life Span Biosciences). In contrast to other Srebp-1 antibodies (Santa Cruz Biotechnology), this antibody was found to be suitable for IHC. In control animals, mild staining of both the cytoplasm as well as of nucleus of the kidney tubules, indicative of basal expression of Srebp, was observed (Fig. 3*I*). Minimal staining of the glomerular cells was observed, which authenticated specificity of the antibody. Following HFD

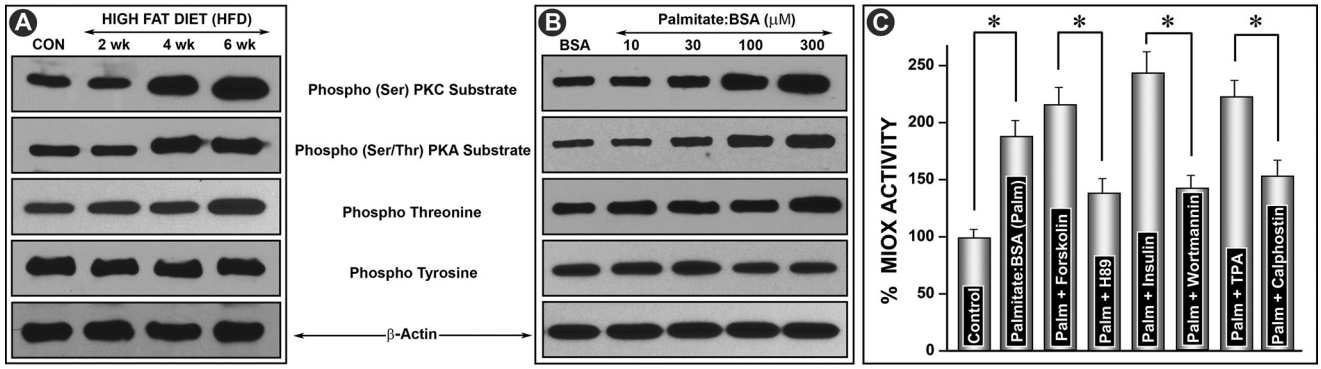

FIGURE 2. **Modulation of phosphorylation of Miox and its activity by HFD and albumin-bound fatty acids.** Kidney homogenates or cellular lysates were immunoprecipitated with substrate-specific phosphoantibodies to PKA (Ser/Thr) and PKC (Ser) and to phosphothreonine and phosphotyrosine residues followed by Western blot analyses with anti-Miox antibody. A time-dependent (2–6 weeks) increased phosphorylation was observed with phosphoantibodies directed against serine and threonine residues (*A*). Similarly, a dose-dependent increase in the phosphorylation at serine and threonine residues was observed in cells treated with various concentrations of palmitate/BSA (*B*). No increase was observed in samples immunoprecipitated with anti-phosphotyrosine antibody. Concomitant treatment with palmitate/BSA and activators of PKA (forskolin), PDK/PI3K (insulin), and PKC (TPA) further increased the Miox activity (*C*). Concomitant treatment with respective inhibitors, *i.e.* H89 (PKA), wortmannin (PI3K), and calphostin (PKC), reduced the activity below the levels induced by palmitate/BSA alone, confirming that fatty acid-induced activity is phosphorylation-dependent (*C*). *, $p < 0.01$ *versus* control or inhibitor *versus* activator $n = 4$.

administration, a remarkable increase in the expression in renal proximal tubules was observed (Fig. 3*J*). Intriguingly, increased expression was seen in both cytoplasmic and nuclear (Fig. 3, *I versus J, arrowheads*) compartments of the tubular cells, although there was a very mild increase in glomerular cells. This suggested a specific Srebp1 response following HFD that is selectively confined to tubular cells. In aggregate, these observations suggested responsiveness of Miox and Srebp expression to insulin as well as fatty acids, and this led us to examine the promoter characteristics of *miox*.

Effect of Palmitate/BSA on miox Promoter Activity and Binding of Srebp to the SRE of Its Promoter—To explore mechanisms that up-regulate expression of Miox by palmitate/BSA, human *miox* gene upstream of the open reading frame (ORF) was cloned by genomic PCR amplification, and it was used for promoter activity analyses. First, three constructs were generated spanning *miox* gene −1,500 bp upstream of ORF. The construct spanning the entire region had maximum *miox* basal promoter activity, as shown schematically (Fig. 4*A*). This construct was enriched with E-box sites and at the same time was inclusive of multiple SRE sites. The SRE and E-box motifs (CANNTG) congregated at −1047 to −1499 in the *miox* promoter region. A total of seven SRE motifs were localized to −1,499- (GTCCCA), −1,328- (AGGGGC), −1,271- (GGTGGTGGA), −1,196- (TTAAAT), −1,137- (CTTGTT), −1,090- (AAGCCCA), and −1,047- (CACCCCAC) bp regions. In addition, a mutant construct was generated by modifying the SRE sites by site-directed mutagenesis. All four constructs were transfected into HK-2 cells and also co-transfected with the luciferase constructs to measure the luciferase activity. The basal activity was designated as one, and following palmitate/BSA treatment a variable increase in luciferase activity was observed in all the constructs (Fig. 4*B*). The highest increase in activity (~2-fold) was observed in the transfected construct inclusive of E-box and SRE sites. A marginal increase in activity in HK-2 cells transfected with the mutant construct was observed, which indicated that responsiveness of the *miox* promoter to fatty acids is mediated via the SRE sites. This suggested that Srebp, a basic helix-loop-helix-leucine zipper transcription factor that is known to regulate cholesterol biosynthesis and fatty acid metabolism (33–35), can potentially bind to the promoter region of *miox* and modulate its transcription following palmitate/BSA treatment.

To investigate the existence of SRE sites and binding of Srebp1 with the *miox* promoter, electrophoretic mobility shift assays (EMSA) were performed, using nuclear extracts of HK-2 cells in a non-denaturing minigel system. The reaction mixtures included nuclear extracts, unlabeled cold or biotin-labeled double-stranded oligonucleotide probes (−1048 to −1017 bp), or an anti-Srebp-1 antibody. A shifted band was seen in the biotin-labeled oligonucleotide probe (Fig. 4*C*, *lower arrow, middle lane*). The unlabeled cold oligonucleotide probe effectively competed with the labeled probe in nuclear protein reaction mixture because the shifted band disappeared (Fig. 4*C*, *left lane*); a nonspecific low molecular band and free labeled oligonucleotides were seen in this lane. With the inclusion of anti-Srebp1 antibody in reaction mixture, a super-shifted band to a higher molecular weight was seen, which suggested the formation of the SRE-oligonucleotide-nuclear protein complex and existence of an Srebp1-binding SRE site in the promoter region of the *miox* gene (Fig. 4*C*, *upper arrow, right lane*). To investigate whether binding of Srebp1 with the *miox* promoter was dose-dependent, ChIP assays were carried out on HK-2 cells treated with BSA or palmitate/BSA (10–100 μM) for 24 h. ChIP PCR products were amplified from input-positive control (Fig. 4*D*, *Input*), a negative control normal rabbit IgG (*Neg*), and an antibody specific for Srebp1 (*ChIP*). ChIP assays were followed by PCR analyses of the SRE region (−1499 to −1229) with the expected PCR product size of 271 bp. A dose-dependent increase in binding of Srebp1 to SRE sites was observed following palmitate/BSA treatment (Fig. 4*D*). No band was seen in negative control samples where normal rabbit IgG was substituted for Srebp1 antibody.

Finally, to ensure the functionality of *srebp1* in transfected cells that this transcription factor can modulate Miox expression a 1,500-bp Srebp1 cDNA was cloned into the pcDNA3.1/V5-His-TOPO. This vector was transfected into cells by utilizing FuGENE 6, and stable transfectants were gen-

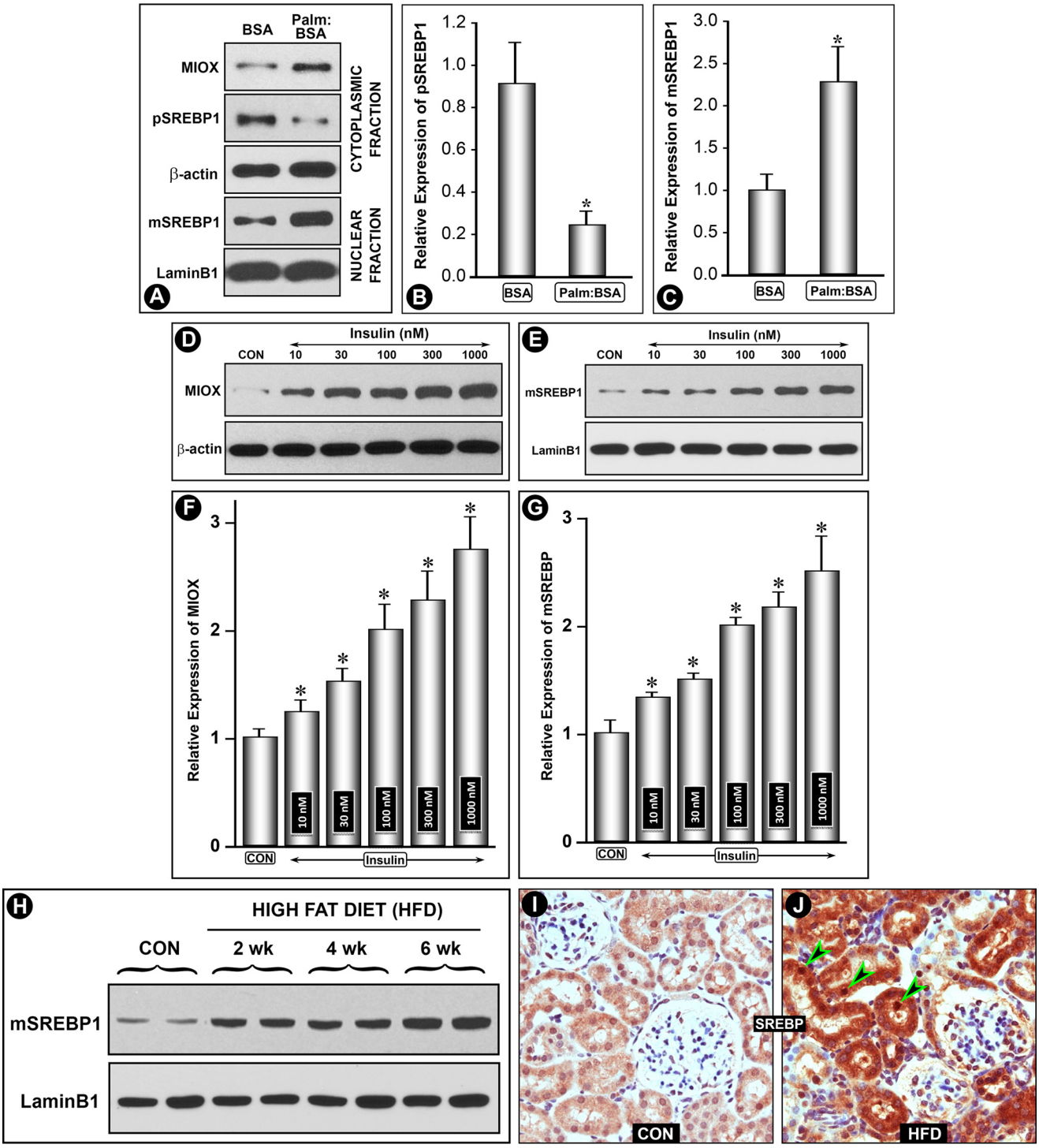

FIGURE 3. **Modulation of Miox and Srebp1 expression by hyperlipidemia, palmitate/BSA, and insulin.** Treatment of HK-2 cells with palmitate/BSA (*Palm/BSA*) (100 μM) increased Miox expression with a concomitant decrease in membrane-bound precursor form of pre-Srebp1 (pSrebp1, 120 kDa) in the cytoplasmic fraction and a simultaneous recruitment and cleavage mature form (mSrebp1, 68 kDa) translocated into the nucleus (*A–C*). No change in the expression of β-actin or laminB1 was observed. In view of the fact that Srebp1 is activated and is associated with excessive secretion of insulin, expression of Miox and mSrebp1 was determined. A dose-dependent increase in expression of Miox and mSrebp1 was observed following insulin (10–1,000 nM) treatment, suggesting a temporal relationship between the up-regulation of Miox and translocation/expression of mSrebp1 (*D–G*). *Con,* control. The *in vivo* results were similar to those seen in cultured cells exposed to palmitate/BSA. HFD administration over a period of 6 weeks to mice resulted in a time-dependent up-regulation of mSrebp1 (*H*). IHC studies confirmed the up-regulation of Srebp in renal proximal tubules, both in cytoplasmic and nuclear fractions (*I* and *J, arrowheads*). *, $p < 0.01$ *versus* control, $n = 4$.

erated. Expression of transfected Srebp1, His protein, and Miox was confirmed by Western blot analysis using antibodies directed against anti-His tag, anti-Srebp1, and anti-Miox. His-tagged antibody could confirm the presence of His fusion protein in cells transfected with pcDNA3.1/V5-His TOPO *srebp1*, although no band was seen in cells transfected with empty vector (Fig. 4*E*). The pcDNA-transfected cells also yielded an increased expression of both Srebp1 and Miox, suggesting

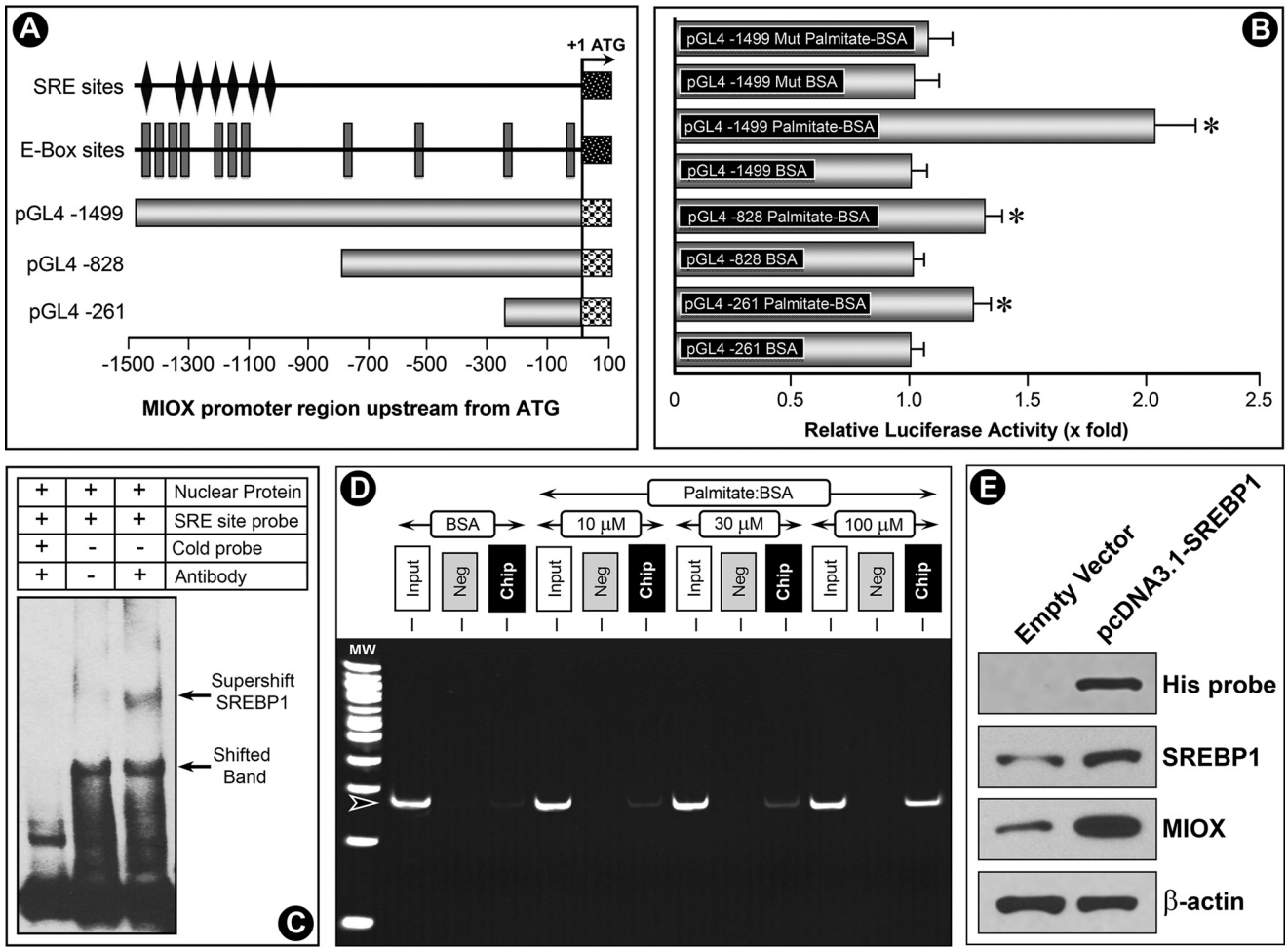

FIGURE 4. **Modulation of *miox* promoter activity by palmitate/BSA and characterization of binding of Srebp to SRE.** Three constructs were generated spanning the *miox* gene −1500 bp upstream of ORF, and one spanning the entire region had maximum *miox* basal promoter activity (*A*). This construct was populated with E-box sites and multiple SRE sites. A mutant construct was generated by modifying the SRE sites by site-directed mutagenesis. The constructs were transfected into HK-2 cells and co-transfected with the luciferase constructs to measure the luciferase activity. Basal promoter activity was designated as 1, and following the palmitate/BSA treatment a variable increase in luciferase activity was observed in all constructs (*B*). The highest palmitate-induced increase in activity (~2-fold) was observed in the transfected construct inclusive of E-box and SRE sites. A marginal increase in activity in HK-2 cells transfected with mutant construct was observed, which indicated that the responsiveness of *miox* promoter to fatty acids is mediated via SRE sites. EMSA revealed a shifted band where a biotin-labeled oligonucleotide probe was included in the incubation mixture (*C, lower arrow, middle lane*). Unlabeled cold oligonucleotides probe effectively competed because the shifted band disappeared (*C, left lane*). With inclusion of anti-Srebp1 antibody in the reaction mixture, a super-shifted band to a higher molecular weight was seen (*C, upper arrow, right lane*). To investigate whether binding of Srebp1 with the *miox* promoter was dose-dependent, ChIP assays followed by PCR were performed following palmitate/BSA treatment with an expected PCR product size of 271 bp. A dose-dependent increase in the binding of Srebp1 to SRE sites was observed following palmitate/BSA treatment (*D*). No band was seen in negative control samples where normal rabbit IgG was substituted for Srebp1 antibody. Functionality of Srebp1 in transfected cells was confirmed by Western blot analysis using antibodies directed against His tag, Srebp1, and Miox. His-tagged antibody could confirm the presence of His fusion protein in cells transfected with pcDNA3.1/V5-His TOPO Srebp1, although no band was seen in cells transfected with empty vector (*E*). The pcDNA-transfected cells also yielded an increased expression of both Srebp1 and Miox, suggesting Srebp1 is functional in transfected cells and can modulate Miox expression (*E*). These experiments validated that fatty acids up-regulate Srebp1, which then binds to the *miox* promoter and modulates *miox* transcription. *, $p < 0.01$ *versus* control, $n = 4$.

Srebp1 is functional in transfected cells and can modulate the Miox expression. This validated the findings of promoter analyses studies, which indicated that fatty acids up-regulate Srebp1 and then it binds to *miox* promoter and modulates *miox* transcription (Fig. 4*E*).

Effect of HFD Diet on Srebp1, Tubular Cytoplasmic and Nuclear Alterations, Senescence, Apoptosis, and Urinary Protein Excretion in Mice and Rats—Because studies detailing the effect of HFD on kidney tubules in the literature are limited, we therefore examined cytoplasmic and nuclear changes in the context of Srebp-1 and Miox pathobiology. We examined both rat and mouse kidneys to assess the morphologic and biochemical differences and similarities between two species, utilizing various IHC markers. Overall, major changes were seen in the metabolically active tubular compartment of the kidney in both the species. In mice, notable morphologic changes were observed in the tubular compartment in kidney sections stained with periodic acid-Schiff. There was a partial loss of the pink staining luminal brush border (Fig. 5, *A versus B, arrows*) with extrusion and falling of nuclei from tubular cells (*arrowheads*). Bcl2 expression was decreased while conversely that of apoptogenic Bax was remarkably increased in tubular cells (Fig. 5, *C–F*). Damage to tubular nuclear DNA was assessed by IHC staining with anti-pH2AX antibody that localizes the phosphorylated form of histone variant H2AX at the Ser^{139} residue. Many nuclei with prominent pH2AX staining were observed in

kidney tubules of mice fed the HFD (Fig. 5, *G versus H*, *arrowheads*). Tubular damage was reflected by pathophysiologic changes as well. There was an increased urinary excretion of low molecular proteins ranging 30–45 kDa (Fig. 5*Q*, *arrows*). Proteinuria was time-dependent for up to 6 weeks, and a mild increase in albumin excretion was also observed, suggesting that glomerular damage is less at this time interval. Likewise, changes were seen in kidney tubules of rats fed an HFD. A tremendous increase in the expression of Miox in kidney tubules was observed, and it had an identical spatio-temporal

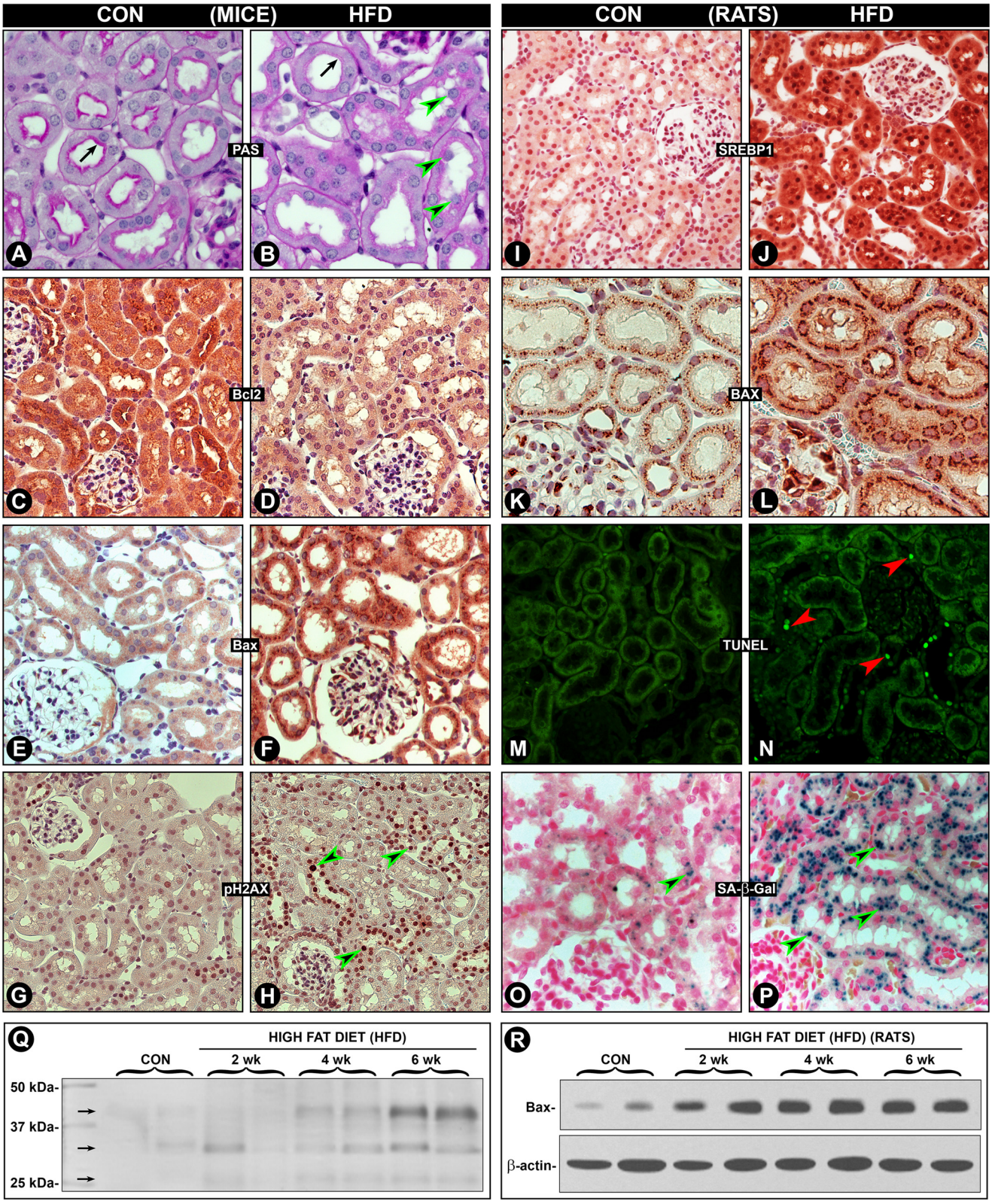

distribution in the tubular compartment as seen in mice following 2–6 weeks of HFD administration (Fig. 1, *A* and *B*). Srebp1 expression was increased in both the cytosolic and nuclear compartment, as reflected by increased antibody staining in cytoplasm and nuclei (Fig. 5, *I versus J*). This suggested that an HFD-induced induction of Miox is mediated via Srebp1 transcription factor in rats as well. Associated with it was an increased expression of apoptogenic Bax, and it had both cytoplasmic and perinuclear distribution (Fig. 5, *K versus L*). Increased expression of Bax following HFD administration was time-dependent up to 6 weeks, as assessed by immunoblot analyses (Fig. 5*R*). HFD-induced nuclear damage in rats was reflected by an increased degree of apoptosis as highlighted by TUNEL staining (Fig. 5, *M versus N*). In view of the HFD-induced cellular and nuclear changes, the replicative capacity of tubular cells was investigated by using SA-β-Gal activity marker. Strikingly, a marked increase in SA-β-Gal staining was observed (Fig. 5, *O versus P, arrowheads*), suggesting that HFD administration has affected the overall homoeostasis of renal tubules concomitant with increased expression of Miox and Srebp1.

Effect of Rapamycin on HFD-induced Miox Expression and Associated Changes in the Renal Tubules—Because mammalian target of rapamycin is activated in states of obesity, studies were carried out *in vivo* to assess the effect of rapamycin on HFD-induced expression of Miox, Srebp1, and changes in biomarkers associated with cytoplasmic or nuclear damage and related functional parameters. Six weeks of HFD administration resulted in a significant increase in body weight, blood glucose, and serum insulin levels (Fig. 6, *A*, *C,* and *D*). In overweight animals, obesity was mainly due to an increase in abdominal fat, and these changes were normalized to basal levels with concomitant administration of rapamycin. Along with an increase in abdominal fat, there was an ~40% increase in serum cholesterol levels in mice fed an HFD, *i.e.* 134 ± 15.56 *versus* 188 ± 8.94 mg/dl, which was reversed with rapamycin treatment. Also, pathologic changes, *i.e.* loss of proximal tubular brush border and extrusion of nuclei (*arrowheads*) were restored to normal by administration of rapamycin (Fig. 6, *E–G*). Interestingly, HFD-induced expressions of Miox (mRNA and protein), Bax, and pH2AX were restored to basal expression following rapamycin treatment as well (Fig. 6, *B* and *H–P*), suggesting a relationship between obesity, Miox expression, apoptogenic Bax, nuclear DNA damage, reflected by pH2AX staining, and blood glucose, cholesterol, and insulin levels, parameters that are conceivably deranged in metabolic syndrome.

Effect of Rapamycin on Palmitate/BSA-induced Miox, Srebp1, and p53 Expression and Apoptosis in Renal Tubular Cells—To establish a mechanistic causal relationship between fatty acid injury leading to up-regulated expression of Miox via transcription factor Srebp1, *in vitro* experiments were performed using HK-2 cells. A basal expression of Miox and Srebp1 was observed in HK-2 cells treated with BSA (Fig. 7, *A* and *D*). With the treatment of palmitate/BSA (100 μM), there was a marked simultaneous increase in expression of Miox and Srebp1 (Fig. 7, *B* and *E*), and it was dramatically reduced with rapamycin treatment (Fig. 7, *C* and *F*). At high magnification, the expression of Srebp1 was equally localized to both the cytoplasm and nucleus under basal conditions, and it was notably increased in the nuclear compartment following palmitate/BSA treatment (Fig. 7, *G* and *H*, *arrowhead*). Nuclear expression was remarkably reduced following rapamycin, suggesting that the mammalian target of rapamycin pathway is involved in up-regulation of Miox and Srebp1 (Fig. 7*I*). Along with an increase in expression of Miox and Srebp1, there was a concomitant increase of apoptosis following palmitate/BSA treatment, which was notably reduced by rapamycin, as assessed by the TUNEL method. TO-PRO-3 dye was used as a nuclear stain; it yields a red color and cells undergoing apoptosis acquire a yellow color (Fig. 7, *J–L*). Apoptosis observed was most likely triggered by p53 because there was an increased expression of p53, which could be inhibited by rapamycin treatment, as indicated by the immunoblots (Fig. 7*M*). Interestingly, this increase and decrease of p53 was congruent with expression of Miox following various treatments. To elucidate a direct causal relationship between Miox and Srebp1, siRNA experiments were performed. With *srebp1* siRNA treatment, Miox expression was dramatically reduced in palmitate/BSA-treated cells, although scrambled oligonucleotide had no effect (Fig. 7*N*). Specificity of *srebp1* siRNA was confirmed by measuring mRNA expression. *srebp1* siRNA caused a remarkable reduction in expression of Srebp1 in palmitate/BSA-treated cells, although a scrambled oligonucleotide had a minimal effect (Fig. 7*O*). Next, we proceeded to address the question of whether Srebp-1-induced Miox expression leads to changes in cellular redox.

Effect of Palmitate/BSA or HFD-induced Perturbations in Cellular Redox in Renal Tubular Cells—Cells were treated with different concentrations of palmitate/BSA for 24 h, and cellular ROS generation was assessed by CM-H_2DCF-DA staining followed by flow cytometric analysis. A dose-dependent increase in mean fluorescence intensity (MFI) related to DCF-DA staining was observed within the concentration range of 30–300 μM palmitate/BSA (Fig. 8*A*). Likewise a dose-dependent increase in mitochondrial ROS was observed following treatment with palmitate/BSA, as assessed by MitoSOX staining and flow cytometry (Fig. 8*B*). These *in vitro* observations were confirmed by *in vivo* experiments. To assess the effect of an HFD on cellular redox, kidney sections from mice fed with control and an

FIGURE 5. **Modulation of Srebp1 expression, cytoplasmic and nuclear alterations, senescence, apoptosis, and urinary protein excretion in mice and rats by HFD.** Studies were performed to assess the effect of HFD on morphologic and biochemical changes in both the species in metabolically active tubular compartment. In mice, a loss of the pink staining luminal brush border (*A versus B*, *arrows*) with extrusion of nuclei of tubular cells was observed (*arrowheads*). The Bcl2 expression was decreased, and that of apoptogenic Bax was increased (*C–F*). Anti-pH2AX-associated nuclear staining (reflective of nuclear DNA damage) was seen in many tubular nuclei of mice fed an HFD (*G versus H*, *arrowheads*). Tubular damage was also reflected in increased time-dependent urinary excretion of low molecular proteins ranging from 30 to 45 kDa (*Q*, *arrows*). Some of the changes seen in kidney tubules of rats fed with HFD are depicted here. Identical to the Miox expression, an increased expression of Srebp1 (*I versus J*) and BAX (*K versus L*) was observed. The increased expression of Bax was time dependent (*R*). This was associated with increased apoptosis, as highlighted by TUNEL staining (*M versus N*). In addition, a marked increase in SA-β-Gal staining was observed (*O versus P, arrowheads*), suggesting an increased replicative capacity of tubular cells following HFD-induced cellular damage. Overall, these changes suggest that HFD adversely affect the cellular homeostasis in both the species.

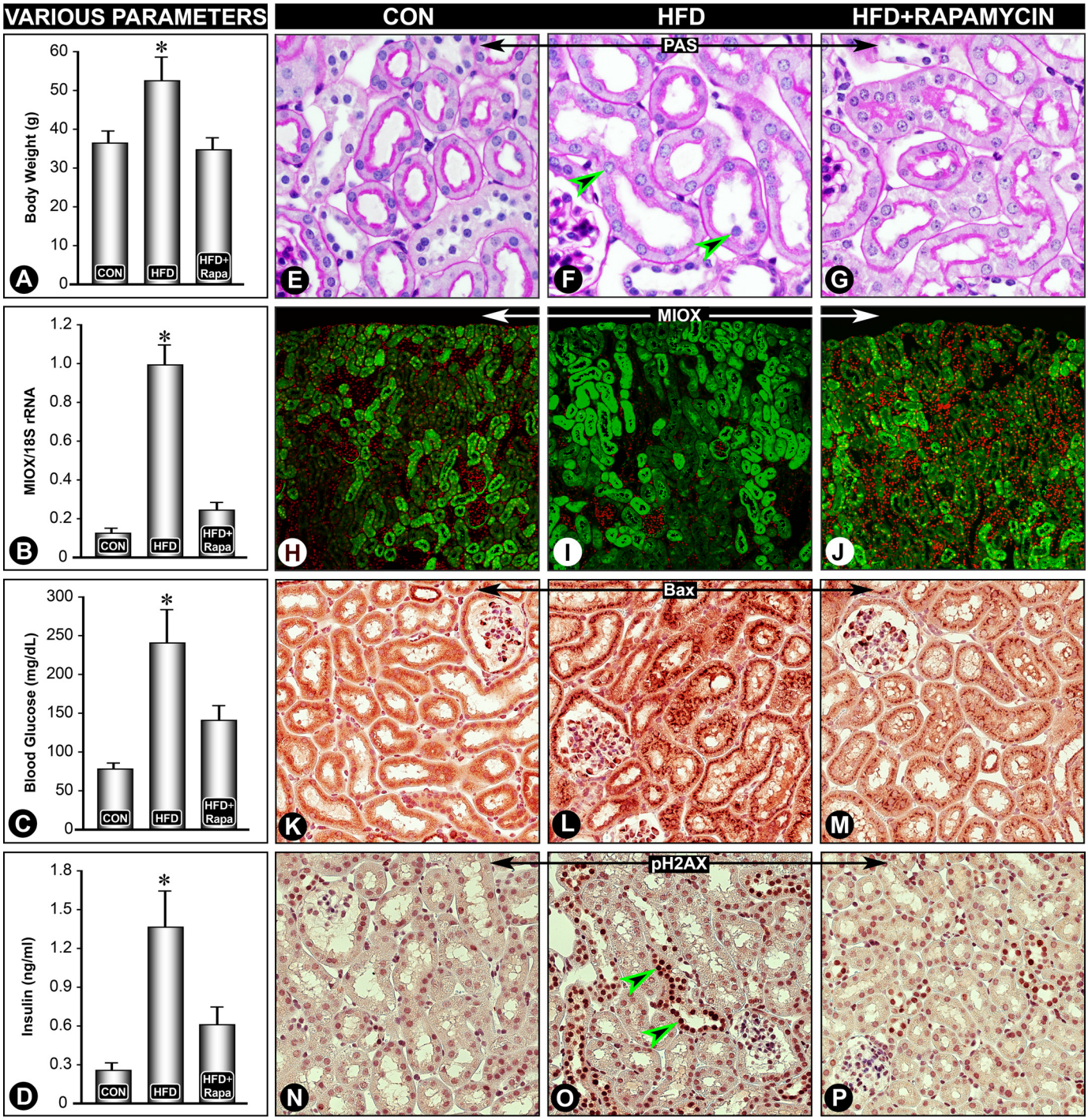

FIGURE 6. **Rapamycin reverses HFD-induced Miox expression and associated changes in the renal tubules.** A significant increase in body weight, blood glucose, and serum insulin levels was observed following HFD administration, and it was reduced following rapamycin treatment (*A*, *C*, and *D*). HFD-induced pathologic changes, *i.e.* loss of proximal tubular brush border and extrusion of the nuclei (*arrowheads*) were reversed by rapamycin treatment (*E–G*). Also, the expression of Miox (mRNA and protein), Bax, and pH2AX was restored to basal levels following rapamycin treatment (*B* and *H–P*). *, $p < 0.01$ *versus* control, $n = 4$.

HFD were processed for CM-H_2DCF-DA and DHE staining. A notable increase in both CM-H_2DCF-DA and DHE staining was observed in kidney sections of mice fed an HFD, suggesting increased intracellular levels of ROS (Fig. 8, *C* and *E versus D* and *F*). DCF staining was mainly confined to the cytoplasm of the tubules (Fig. 8*D*). Glomerular cells did not yield any distinct notable increase in DCF staining. DHE staining was also confined to the tubular compartment, and it was seen exclusively localized to nuclei (Fig. 8*F*). No notable DHE staining was seen in kidney sections of mice fed a normal diet (Fig. 8*E*).

Effect of srebp1 and miox siRNA on Palmitate/BSA-induced Perturbations in Cellular Redox of Renal Tubular Cells—Keeping in view that HFD administration to mice or palmitate/BSA treatment to HK-2 cells leads to increased Miox expression, we addressed the question whether increased generation of ROS is specific to Miox and is mediated via Srebp1 transcription fac-

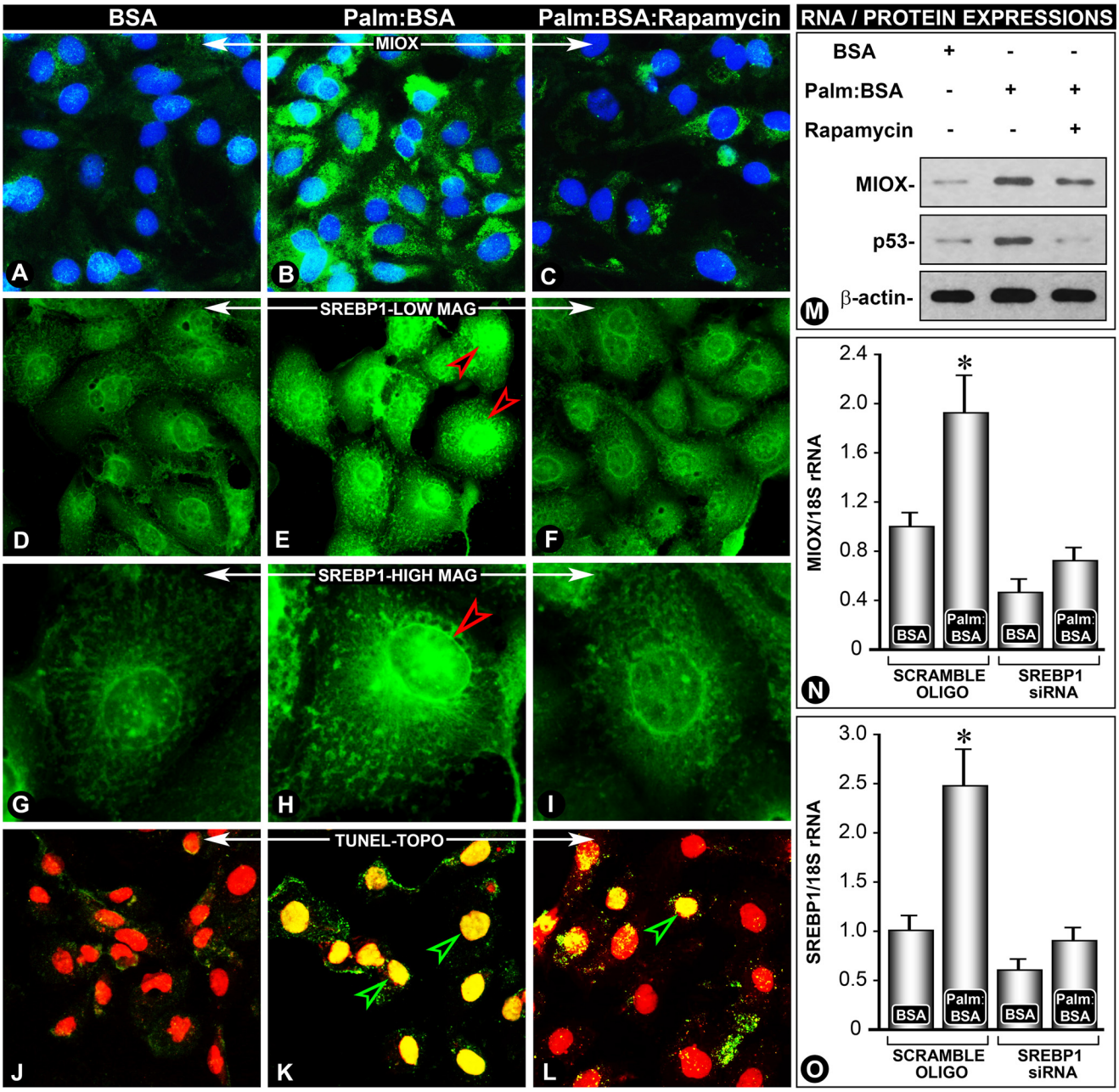

FIGURE 7. **Rapamycin reverses palmitate/BSA-induced Miox, Srebp1, and p53 expression and apoptosis in renal tubular cells.** A notable increase in the expression of Miox and Srebp1 was observed following treatment with palmitate/BSA compared with BSA-treated cells alone (*B* and *E versus A* and *D*). The increase was predominantly confined to the nuclear fraction (*G* and *H, arrowhead*). The increased expression of Miox and Srebp1 was reduced with rapamycin treatment (*C, F,* and *I*), suggesting that the mTOR pathway is involved in the up-regulation of Miox and Srebp. Associated with the increased expression of Miox and Srebp1, a concomitant increase of apoptosis (*K, yellow*-colored nuclei) was seen, and it was reduced by rapamycin treatment, as assessed by the TUNEL assay (TO-PRO-3 dye) (*L, red*-colored nuclei). Normally, the intact nuclei yield red fluorescence after staining with this dye (*J*).The apoptosis observed was most likely mediated by p53, and its increased expression was also reduced by rapamycin (*M*). A causal relationship between Miox and Srebp1 was established by siRNA experiments where *srebp1* siRNA treatment reduced *miox* as well as *srebp1* mRNA expression (*N* and *O*). *, $p < 0.01$ *versus* control, $n = 4$.

tor. HK-2 cells treated with palmitate/BSA were subjected to siRNA gene disruption, and then they were stained with CM-H_2DCF-DA. Following that, ROS levels were monitored by flow cytometry and fluorescent microscopy. A significant increase in DCF staining and MFI following palmitate/BSA treatment was observed (Fig. 9, *A versus B*). However, following *srebp1* siRNA or *miox* siRNA treatment the palmitate/BSA-induced increase in MFI was notably reduced (Fig. 9, *C–E*). The reduction in MFI was comparable following the *miox* siRNA or *srebp1* siRNA treatment. Fluorescent microscopy of HK-2 cells subjected to various treatments confirmed the findings of flow cytometric analyses. By fluorescent microscopy a notable increase in intensity of staining was observed following palmitate/BSA treatment (Fig. 9, *F versus G*). Both the *srebp1* siRNA and miox siRNA treatments remarkably reduced intensity of fluorescence, suggesting that palmitate/BSA-induced ROS perturbations are specific to Miox and are mediated via Srebp1 (Fig. 9, *H* and *I*).

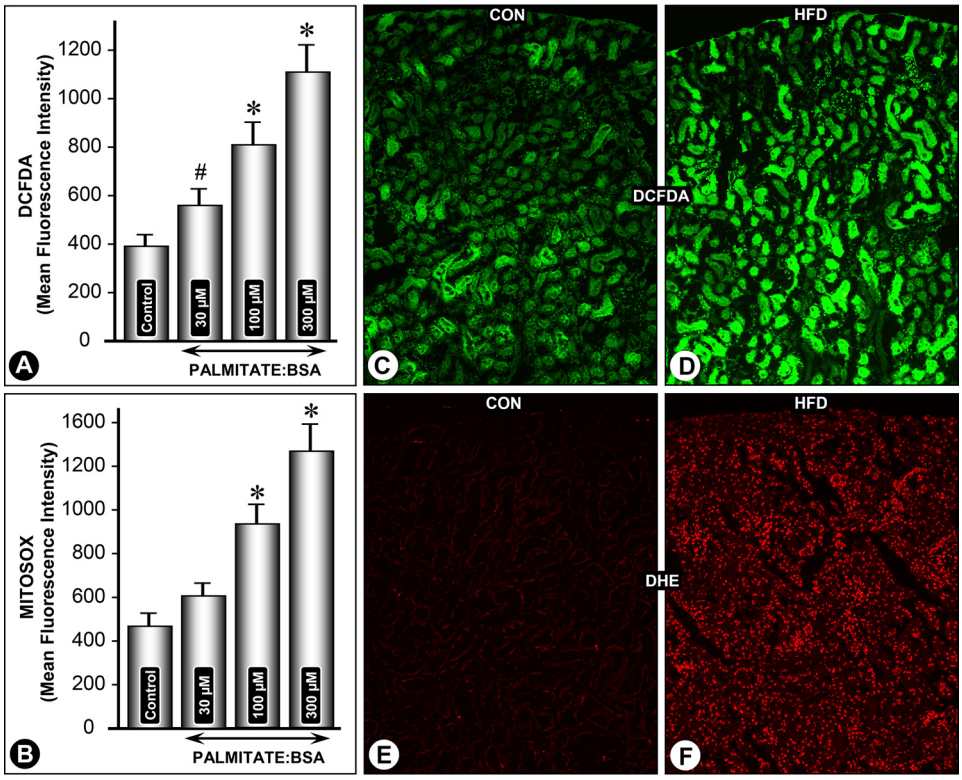

FIGURE 8. **Palmitate/BSA and HFD-induced perturbations in cellular redox in renal tubular cells.** A dose-dependent increase in MFI related to CM-H_2DCF-DA and MitoSOX staining was observed in HK-2 cells following palmitate/BSA treatment (*A* and *B*). Likewise, a notable increase in both CM-H_2DCF-DA and DHE staining was observed in kidney sections of mice fed an HFD (*D* and *F versus C* and *E*). DCF staining was mainly confined to the cytoplasm of tubules, although the glomeruli were unaffected. *, $p < 0.01$ *versus* control, $n = 4$.

Discussion

The results of this investigation highlight that in states of obesity there is an up-regulation of a kidney-specific metabolic enzyme, *i.e.* Miox, with activation of the glucuronate-xylulose pathway in which *myo*-inositol via a series of reactions gets converted into xylulose and ribulose along with the generation of ROS. The latter would likely adversely affect the pathobiology of the tubulo-interstitial compartment of the kidney. In such a setting, the tubulo-interstitial injury besides the glomerular injury would be reflected in compromised renal functions. In this regard, currently obesity has emerged as a significant risk factor, independent of diabetes and hypertension, in the progression of chronic kidney disease on a long term basis (36). So far most of the mechanistic studies concerning development of chronic kidney disease in states of obesity have focused on the glomerular compartment, especially on the podocyte, whereas the proximal tubular cell/compartment has not received much attention, although it is equally affected by various adverse metabolic assaults (6, 36, 37).

Previously, we reported the status of Miox in the context of type 1 and 2 models of diabetes while focusing on the biology of the proximal tubular compartment (20, 22, 24). Because this enzyme is conserved across various species lines, we utilized different proximal tubular cell lines and mice and rats to investigate its pathobiology in states of obesity and exposure of cells to albumin-bound fatty acids. The latter strategy would mimic the *in vivo* renal disease states, such as nephrosis, where the tubular cells are subjected to assault by the filtered albumin-bound fatty acids. Like in type 1 or 2 diabetes the mice receiving the HFD had a marked time-dependent (1–6 weeks) increased expression of Miox and activity in the proximal tubules, although the glomeruli were unaffected (Fig. 1). One may regard the time-dependent increase in expression to be dose-dependent as well because cholesterol levels gradually increased with time being significantly high at 6 weeks. In fact, *in vitro* exposure of palmitate/BSA induced an increased expression and activity of Miox in LLC-PK1 cells in a dose-dependent manner. The question of toxicity of palmitate/BSA leading to cellular disintegration was ruled out because Bax expression was concomitantly increased up to a concentration range of 300 μM. Miox activity was reduced to basal levels with the treatment of λ-PPase, suggesting that phosphorylation may be essential for the activity of this enzyme. Phosphorylation can induce a conformational change in the protein to associate or dissociate with other proteins or increase or decrease substrate affinity and thereby reduce or accentuate the activity of a given enzyme (38, 39). Kinase-induced phosphorylation or phosphatase-mediated dephosphorylation processes target serine, threonine, or tyrosine residues. All of these potential sites are included in the Miox protein and are amenable to phosphorylation in different biologic processes thereby increasing its expression and activity (22). As in the diabetic state or the cells under high glucose ambience, there was an increased expression and activity at the serine or threonine residues following HFD administration or treatment of LLC-PK1 cells with palmitate/BSA (Fig. 2). The role of phosphorylation in regulation of

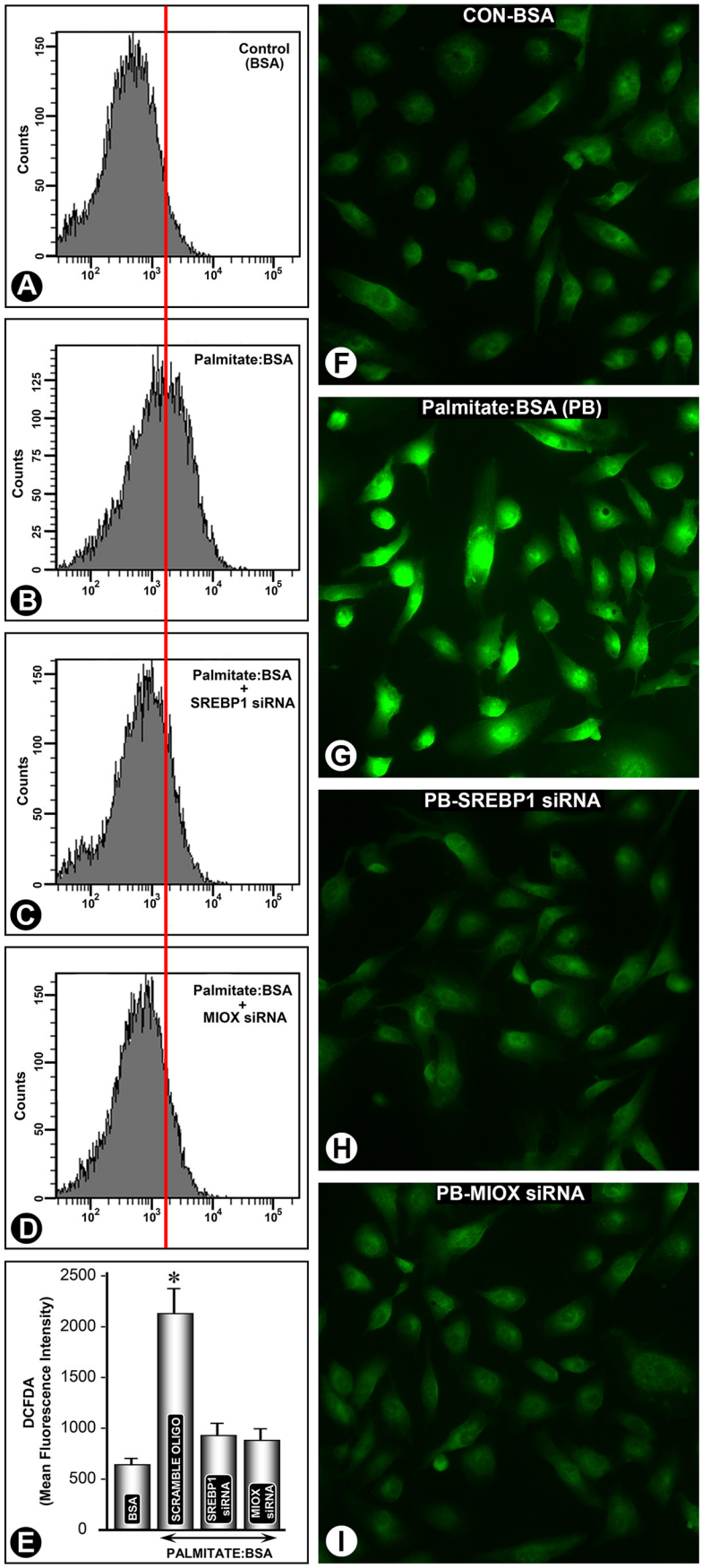
Control (BSA)
Counts
A
Palmitate:BSA
B
Palmitate:BSA + SREBP1 siRNA
C
Palmitate:BSA + MIOX siRNA
D
DCFDA (Mean Fluorescence Intensity)
BSA
SCRAMBLE OLIGO
SREBP1 siRNA
MIOX siRNA
PALMITATE:BSA
E
CON-BSA
F
Palmitate:BSA (PB)
G
PB-SREBP1 siRNA
H
PB-MIOX siRNA
I

Miox activity by fatty acids was further substantiated by the fact that various activators or inhibitors of PKC, PKA, and PDk1 were able to boost or inhibit palmitate/BSA-induced Miox activity. Interestingly, because insulin also could remarkably induce Miox activity, this would suggest its significance and a link in various pathobiologic processes like diabetes and obesity, the latter relating to perturbation in the fatty acid metabolism.

A number of genes that are involved in the synthesis of fatty acids, cholesterol, triglycerides and phospholipids, are regulated by transcription factors known as Srebps (32–35). They belong to the basic helix-loop-helix-leucine zipper family of transcription factors, and they are bound to the endoplasmic reticulum in an inactive precursor form, *i.e.* pSrebp. Upon activation by various stimuli, *e.g.* hyperinsulinemia, Srebp is escorted by Srebp cleavage-activating protein into the Golgi apparatus where it undergoes successive cleavage by site-1 protease and site-2 protease. The mature form (mSrebp) translocates into the nucleus and binds to SRE to initiate transcription of various genes (32–35). Given the above considerations, we investigated whether HFD-induced up-regulation of Miox was mediated by insulin via utilizing Srebp transcription factors. In line with this notion, we observed that palmitate/BSA increased the expression of mSrebp1 concomitant with the up-regulation of Miox and decreased expression of pSrebp1 (Fig. 3). Similarly, the HFD diet increased the expression of mSrebp1 in a proximal tubular compartment (Fig. 3). However, no significant increase in Srebp1 expression or glomerulosclerosis was observed following HFD administration. Conceivably, these differences may be related to the duration of HFD administration, *i.e.* 6 weeks *versus* 12 weeks or use of different strains of mice, *i.e.* CD1 *versus* C57BL/6J (40). Insulin is also known to increase the expression of Srebp1 in adipocytes (30), and likewise a dose-dependent increase in HK-2 cells with a concomitant up-regulation of Miox was also observed (Fig. 3).

Collectively, the above observations suggest that the biology of Srebp1 and Miox is interlinked in states of high insulin or fatty acid ambience. This led us to investigate the transcriptional regulation of Miox. The *miox* promoter included multiple SREs and E-box motifs localized from −1047 to −1099 bp (Fig. 4). This suggested that Miox is a potential target candidate of Srebp-1 that has dual DNA-binding specificity (30, 41). Although Srebps have many potential targets, but two well characterized genes to which adipocyte determination- and differentiation-dependent factor 1 (ADD1)/Srebp1, with dual DNA-binding specificity, can bind include fatty-acid synthase and leptin. Incidentally, both are involved in fatty acid metabolism (30, 42). It is known that many transcription factors bind to the E-box, including TFE3 and USF1, and the latter is involved in the synthesis of fatty acids (43, 44). USF1 and Srebp1 cooperate with one another to regulate the transcription of fatty-acid synthase. Thus, conceivably, USF1 in cooperation with Srebp1 could regulate the transcription of *miox* following HFD administration. Among several *miox* promoter constructs, maximal activity was confined to the construct containing the entire promoter segment inclusive of SREs and E-box motifs. A marked increase in the activity was noted following palmitate/BSA treatment, and it was reduced to basal levels in cells transfected with a mutant construct (Fig. 4). EMSA and ChIP assay further provided the evidence that *miox* transcription is modulated by Srebp1 in states of high fatty acids ambience.

Next, we addressed the question as to which of the genes co-localize with Miox that would be reflective of proximal tubular injury and are induced following HFD administration. Expression studies were carried out both in rats and mice because different species/strains display differential susceptibility to HFD-induced tubular injury (40). In either species there was loss of the proximal tubular brush border with increased low molecular weight proteinuria (Fig. 5). Such low molecular weight proteinuria besides albuminuria has also been reported in states of obesity in children (45). A mild increase in albumin excretion was also observed that may be due to the shorter duration of HFD administration, *i.e.* 6 weeks *versus* 12 weeks (40). HFD administration also induced cellular and nuclear damage, which was readily discernible by TUNEL assay and by delineating the changes in the expression of various genes and markers, *i.e.* Bcl2/Bax and -pH2AX and SA-β-Gal (Fig. 5). Overall, HFD markedly perturbed cellular homeostasis with increased expression of Srebp1 and concomitant up-regulation of Miox. Upstream modulators of Srebp1 are believed to be a group of kinases, including PI3K, Akt/protein kinase, and more importantly another protein kinase known as mTORC1. The latter regulates cell growth by coordinating protein anabolism, nucleotide synthesis, gluconeogenesis, and lipogenesis (46, 47). The mTORC1 is also modulated by 5′-AMP-activated kinase, an enzyme that is a key regulator of carbohydrate as well as lipid metabolism (3, 48). Among these enzymes, mTROC1 seems to rest at the cross-roads of various kinase-mediated signaling pathways and is activated by fatty acids and by states of obesity; and its inhibition by rapamycin leads to amelioration of palmitate-induced endoplasmic reticulum stress and obesity-mediated autophagy insufficiency (48–50). Most of these studies relate to glomerular biology focusing on podocyte injury culminating into glomerulosclerosis, and there are few studies concerning obesity or metabolic syndrome related to tubulo-interstitial injury (45, 51). This investigation addresses an interlinked pathobiology of Miox, mTORC1. and Srebp1 in the context of tubular injury and obesity/metabolic syndrome. It is likely that the scenario that one is dealing with here is reminiscent of metabolic syndrome because the mice had HFD-induced obesity (body weight) and high blood sugar, cholesterol, and insulin levels. Interestingly, these physiologic parameters were normalized along with res-

FIGURE 9. ***srebp1* and *miox* siRNA reduced palmitate/BSA-induced perturbations in cellular redox in renal tubular cells.** A significant increase in MFI, as assessed by flow cytometric analyses, following palmitate/BSA treatment was observed (*B versus A* and *E*). *srebp1* siRNA treatment reduced the MFI (*C* and *E*). Similarly, a reduction in MFI was observed following *miox* siRNA treatment (*D* and *E*). Likewise fluorescent microscopy of HK-2 cells revealed a notable increase in intensity of staining following palmitate/BSA treatment (*G versus F*). Both the *srebp1* siRNA and *miox* siRNA treatments remarkably reduced intensity of fluorescence, suggesting that palmitate/BSA-induced ROS perturbations are specific to *miox* and are mediated via Srebp1 (*H* and *I*). *, $p < 0.01$ *versus* control, $n = 4$.

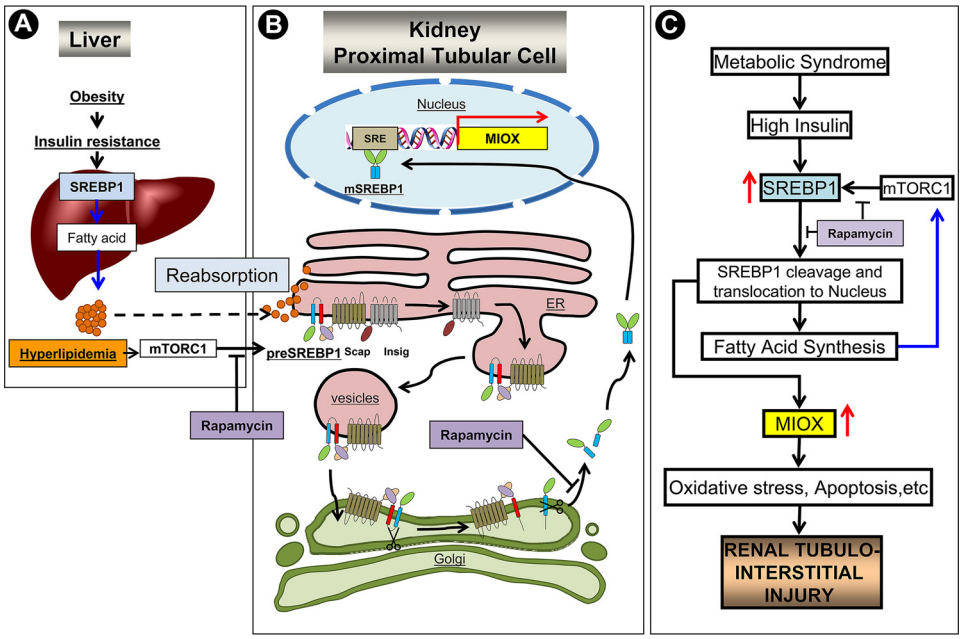

FIGURE 10. **Mechanism(s) of Miox induction leading to tubulo-interstitial injury in states of obesity or metabolic syndrome.** *A,* in states of obesity with the development of insulin resistance, there is an activation of transcription factor, Srebp1, which by modulating fatty-acid synthase (*FAS*) would increase the production of fatty acids in the liver. *B,* conceivably, the fatty acids reabsorbed by the proximal tubular cells activate mTORC1 protein kinase (48–50), which in turn would increase the expression of preSrebp1. The preSrebp1 is escorted by Scap from the endoplasmic reticulum to the Golgi via vesicular transport with simultaneous dissociation of Insig. In the Golgi saccules the preSRBEP1 is successively cleaved by site-1 and -2 proteases to generate a mature form, *i.e.* mSrebp1. The mSrebp1 translocates into the nucleus, binds to SREs, and initiates transcription of *miox*. *C,* summary of signaling events leading up to Miox activation, oxidant stress and thereby tubulo-interstitial injury are depicted. In addition, various steps where rapamycin conceivably can interrupt mTORC1 signaling are also depicted. *ER,* endoplasmic reticulum; *Scap,* Srebp cleavage activating protein; *Insig,* insulin-induced gene; *SRE,* sterol-response elements.

toration of villous architecture of proximal tubules and reduction in expression of Miox and markers of cellular/nuclear damage (Fig. 6). To interlink the biologic relationship between Miox, Srebp1, and mTORC1, the *in vitro* experiments utilizing HK-2 cells, rapamycin, and siRNA techniques were carried out. Treatment of cells with rapamycin concomitantly reduced the palmitate/BSA-induced expression of Miox and Srebp-1 (Fig. 7). Nuclear translocation of Srebp1 was also remarkably reduced, suggesting that inhibition of mTROC1 led to a down-regulation of Miox that is most likely mediated via the Srebp1 transcription factor. The fact that palmitate/BSA-induced Miox and Srebp1 expression was reduced by *srebp1* siRNA would strongly suggest the existence of an mTORC1-Srebp1 signaling pathway that modulates the pathobiology of Miox. In addition, the extent of apoptosis was remarkably reduced by rapamycin, and this process, which influences the regulation of Miox, was conceivably mediated through p53 because the latter's expression was reduced (Fig. 7). The p53 is a redox-active transcription factor that modulates cellular responses in the setting of various stresses that lead to genomic instability and apoptosis (52). With respect to cellular redox, ROS may serve as upstream or downstream modulators of p53 signaling, but a long held view is that ROS are downstream mediators of p53-dependent apoptosis (53).

In view of the above discussion and the fact that overexpression of Miox leads to ROS generation (29), we examined the status of ROS in HFD- or palmitate-induced up-regulation of Miox in proximal tubules. ROS, as assessed by staining with DCF-DA and DHE staining, indicative of hydrogen peroxide and superoxide anion generation, were notably increased in the proximal tubular compartment of kidneys of mice fed an HFD for 6 weeks (Fig. 8). Likewise, in *in vitro* experiments a dose-dependent increase in the mean fluorescence intensity of DCF-DA and MITOSOX following palmitate/BSA treatment was observed, which suggested that most likely the ROS generated are derived from both mitochondrial and cytosolic fractions of HK-2 cells, as assessed by flow cytometric analysis (Fig. 8). Although the generation of ROS followed the up-regulation of Miox, it is worth mentioning here that the *miox* promoter includes both oxidant and anti-oxidant response elements (22). Therefore, it is conceivable that Miox activation may lead to setting up a positive regulatory loop with sustained generation of ROS thus accentuating the oxidant stress in proximal tubules. Moreover, in the kidney the HFD diet-induced generation of ROS is also seen in other organ systems, including skeletal muscle, liver, generalized vasculature, and importantly in adipose tissues (2, 6, 14, 54–57). However, peculiar to the kidney is that the HFD diet-induced ROS generation would be sustained because of unique oxidant response elements in the *miox* promoter. Here, another relevant question that needs to be addressed is whether ROS generation directly relates to increased expression of Srebp1 and Miox and whether this process is specific to the Miox pathobiology? With this in mind, siRNA experiments were performed. Both *srebp1*siRNA and *miox* siRNA reduced the DCF-DA-related mean fluorescence intensity, as measured by flow cytometric analyses, as well as gauged by fluorescence microscopy (Fig. 9). The degree of suppression of ROS generation was comparable following the treatment with either of the siRNAs, suggesting an intertwined pathobiology of Srebp1 and Miox.

In summary, this study elucidates mechanisms involved in HFD- or fatty acid-induced transcriptional, translational, and post-translational regulation of Miox expression as well as its activity. Importantly, this investigation also highlights Miox as a novel target of the transcription factor Srebp1 and a new mTORC1/Srebp1/Miox pathway (Fig. 10) in the generation of ROS culminating into tubulo-interstitial injury in states of obesity.

Author Contributions—T. T., R. K. D., and D. J. performed the experiments and wrote the manuscript. T. D., J. K. R., and Y. S. K. guided the investigation and edited the manuscript.

References

1. Bayliss, G., Weinrauch, L. A., and D'Elia, J. A. (2012) Pathophysiology of obesity-related renal dysfunction contributes to diabetic nephropathy. *Curr. Diab. Rep.* **12,** 440–446
2. Tanner, R. M., Brown, T. M., and Muntner, P. (2012) Epidemiology of obesity, the metabolic syndrome, and chronic kidney disease. *Curr. Hypertens. Rep.* **14,** 152–159
3. Singhal, S. S., Figarola, J., Singhal, J., Reddy, M. A., Liu, X., Berz, D., Natarajan, R., and Awasthi, S. (2013) RLIP76 protein knockdown attenuates obesity due to a high-fat diet. *J. Biol. Chem.* **288,** 23394–23406
4. Gregg, E. W., Li, Y., Wang, J., Burrows, N. R., Ali, M. K., Rolka, D., Williams, D. E., and Geiss, L. (2014) Changes in diabetes-related complications in the United States, 1990–2010. *N. Engl. J. Med.* **370,** 1514–1523
5. Kanwar, Y. S., Sun, L., Xie, P., Liu, F. Y., and Chen, S. (2011) A glimpse of various pathogenetic mechanisms of diabetic nephropathy. *Annu. Rev. Pathol.* **6,** 395–423
6. Redon, J., and Lurbe, E. (2015) The kidney in obesity. *Curr. Hypertens. Rep.* **17,** 555
7. Sahin-Efe, A., Katsikeris, F., and Mantzoros, C. S. (2012) Advances in adipokines. *Metabolism* **61,** 1659–1665
8. Fasshauer, M., and Blüher, M. (2015) Adipokines in health and disease. *Trends Pharmacol. Sci.* **36,** 461–470
9. Tartaglia, L. A., Dembski, M., Weng, X., Deng, N., Culpepper, J., Devos, R., Richards, G. J., Campfield, L. A., Clark, F. T., Deeds, J., Muir, C., Sanker, S., Moriarty, A., Moore, K. J., Smutko, J. S., *et al.* (1995) Identification and expression cloning of a leptin receptor, OB-R. *Cell* **83,** 1263–1271
10. Coleman, D. L. (2010) A historical perspective on leptin. *Nat. Med.* **16,** 1097–1099
11. Lusis, A. J., Attie, A. D., and Reue, K. (2008) Metabolic syndrome: from epidemiology to systems biology. *Nat. Rev. Genet.* **9,** 819–830
12. Giacco, F., and Brownlee, M. (2010) Oxidative stress and diabetic complications. *Circ. Res.* **107,** 1058–1070
13. Vallon, V. (2011) The proximal tubule in the pathophysiology of the diabetic kidney. *Am. J. Physiol. Regul. Integr. Comp. Physiol.* **300,** R1009–R1022
14. Zhang, H. M., Dang, H., Kamat, A., Yeh, C. K., and Zhang, B. X. (2012) Geldanamycin derivative ameliorates high fat diet-induced renal failure in diabetes. *PLoS ONE* **7,** e32746
15. Thomas, M. E., Harris, K. P., Walls, J., Furness, P. N., and Brunskill, N. J. (2002) Fatty acids exacerbate tubulointerstitial injury in protein-overload proteinuria. *Am. J. Physiol. Renal Physiol.* **283,** F640–F647
16. Arici, M., Brown, J., Williams, M., Harris, K. P., Walls, J., and Brunskill, N. J. (2002) Fatty acids carried on albumin modulate proximal tubular cell fibronectin production: a role for protein kinase C. *Nephrol. Dial. Transplant* **17,** 1751–1757
17. Weinberg, J. M. (2006) Lipotoxicity. *Kidney Int.* **70,** 1560–1566
18. Birn, H., and Christensen, E. I. (2006) Renal albumin absorption in physiology and pathology. *Kidney Int.* **69,** 440–449
19. Ruggiero, C., Elks, C. M., Kruger, C., Cleland, E., Addison, K., Noland, R. C., and Stadler, K. (2014) Albumin-bound fatty acids but not albumin itself alter redox balance in tubular epithelial cells and induce a peroxide-mediated redox-sensitive apoptosis. *Am. J. Physiol. Renal Physiol.* **306,** F896–F906
20. Yang, Q., Dixit, B., Wada, J., Tian, Y., Wallner, E. I., Srivastva, S. K., and Kanwar, Y. S. (2000) Identification of a renal-specific oxido-reductase in newborn diabetic mice. *Proc. Natl. Acad. Sci. U.S.A.* **97,** 9896–9901
21. Arner, R. J., Prabhu, K. S., Thompson, J. T., Hildenbrandt, G. R., Liken, A. D., and Reddy, C. C. (2001) myo-Inositol oxygenase: molecular cloning and expression of a unique enzyme that oxidizes myo-inositol and D-chiro-inositol. *Biochem. J.* **360,** 313–320
22. Nayak, B., Kondeti, V. K., Xie, P., Lin, S., Viswakarma, N., Raparia, K., and Kanwar, Y. S. (2011) Transcriptional and post-translational modulation of myo-inositol oxygenase by high glucose and related pathobiological stresses. *J. Biol. Chem.* **286,** 27594–27611
23. Prabhu, K. S., Arner, R. J., Vunta, H., and Reddy, C. C. (2005) Up-regulation of human myo-inositol oxygenase by hyperosmotic stress in renal proximal tubular epithelial cells. *J. Biol. Chem.* **280,** 19895–19901
24. Nayak, B., Xie, P., Akagi, S., Yang, Q., Sun, L., Wada, J., Thakur, A., Danesh, F. R., Chugh, S. S., and Kanwar, Y. S. (2005) Modulation of renal-specific oxidoreductase/myo-inositol oxygenase by high-glucose ambience. *Proc. Natl. Acad. Sci. U.S.A.* **102,** 17952–17957
25. Xie, P., Kondeti, V. K., Lin, S., Haruna, Y., Raparia, K., and Kanwar, Y. S. (2011) Role of extracellular matrix renal tubulo-interstitial nephritis antigen (TINag) in cell survival utilizing integrin (α)vβ3/focal adhesion kinase (FAK)/phosphatidylinositol 3-kinase (PI3K)/protein kinase B-serine/threonine kinase (AKT) signaling pathway. *J. Biol. Chem.* **286,** 34131–34146
26. Debacq-Chainiaux, F., Erusalimsky, J. D., Campisi, J., and Toussaint, O. (2009) Protocols to detect senescence-associated β-galactosidase (SA-βgal) activity, a biomarker of senescent cells in culture and *in vivo*. *Nat. Protoc.* **4,** 1798–1806
27. Cousin, S. P., Hügl, S. R., Wrede, C. E., Kajio, H., Myers, M. G., Jr., and Rhodes, C. J. (2001) Free fatty acid-induced inhibition of glucose and insulin-like growth factor I-induced deoxyribonucleic acid synthesis in the pancreatic beta-cell line INS-1. *Endocrinology* **142,** 229–240
28. Charalampous, F. C., and Lyras, C. (1957) Biochemical studies on inositol. IV. Conversion of inositol to glucuronic acid by rat kidney extracts. *J. Biol. Chem.* **228,** 1–13
29. Xie, P., Sun, L., Oates, P. J., Srivastava, S. K., and Kanwar, Y. S. (2010) Pathobiology of renal-specific oxidoreductase/myo-inositol oxygenase in diabetic nephropathy: its implications in tubulointerstitial fibrosis. *Am. J. Physiol. Renal Physiol.* **298,** F1393–F1404
30. Kim, J. B., Sarraf, P., Wright, M., Yao, K. M., Mueller, E., Solanes, G., Lowell, B. B., and Spiegelman, B. M. (1998) Nutritional and insulin regulation of fatty acid synthetase and leptin gene expression through ADD1/Srebp1. *J. Clin. Invest.* **101,** 1–9
31. Roberts, C. K., Hevener, A. L., and Barnard, R. J. (2013) Metabolic syndrome and insulin resistance: underlying causes and modification by exercise training. *Compr. Physiol.* **3,** 1–58
32. Shimomura, I., Hammer, R. E., Richardson, J. A., Ikemoto, S., Bashmakov, Y., Goldstein, J. L., and Brown, M. S. (1998) Insulin resistance and diabetes mellitus in transgenic mice expressing nuclear Srebp-1c in adipose tissue: model for congenital generalized lipodystrophy. *Genes Dev.* **12,** 3182–3194
33. Yokoyama, C., Wang, X., Briggs, M. R., Admon, A., Wu, J., Hua, X., Goldstein, J. L., and Brown, M. S. (1993) Srebp-1, a basic-helix-loop-helix-leucine zipper protein that controls transcription of the low density lipoprotein receptor gene. *Cell* **75,** 187–197
34. Kim, J. B., and Spiegelman, B. M. (1996) ADD1/Srebp1 promotes adipocyte differentiation and gene expression linked to fatty acid metabolism. *Genes Dev.* **10,** 1096–1107
35. Horton, J. D., Goldstein, J. L., and Brown, M. S. (2002) Srebps: activators of the complete program of cholesterol and fatty acid synthesis in the liver. *J. Clin. Invest.* **109,** 1125–1131
36. Ritz, E., Koleganova, N., and Piecha, G. (2011) Is there an obesity-metabolic syndrome related glomerulopathy? *Curr. Opin. Nephrol. Hypertens.* **20,** 44–49
37. Wickman, C., and Kramer, H. (2013) Obesity and kidney disease: potential mechanisms. *Semin. Nephrol.* **33,** 14–22
38. Narayanan, A., and Jacobson, M. P. (2009) Computational studies of pro-

tein regulation by post-translational phosphorylation. *Curr. Opin. Struct. Biol.* **19,** 156–163
39. Xue, Y., Liu, Z., Cao, J., Ma, Q., Gao, X., Wang, Q., Jin, C., Zhou, Y., Wen, L., and Ren, J. (2011) GPS 2.1: enhanced prediction of kinase-specific phosphorylation sites with an algorithm of motif length selection. *Protein Eng. Des. Sel.* **24,** 255–260
40. Jiang, T., Wang, Z., Proctor, G., Moskowitz, S., Liebman, S. E., Rogers, T., Lucia, M. S., Li, J., and Levi, M. (2005) Diet-induced obesity in C57BL/6J mice causes increased renal lipid accumulation and glomerulosclerosis via a sterol regulatory element-binding protein-1c-dependent pathway. *J. Biol. Chem.* **280,** 32317–32325
41. Kim, J. B., Spotts, G. D., Halvorsen, Y. D., Shih, H. M., Ellenberger, T., Towle, H. C., and Spiegelman, B. M. (1995) Dual DNA binding specificity of ADD1/Srebp1 controlled by a single amino acid in the basic helix-loop-helix domain. *Mol. Cell. Biol.* **15,** 2582–2588
42. Rome, S., Lecomte, V., Meugnier, E., Rieusset, J., Debard, C., Euthine, V., Vidal, H., and Lefai, E. (2008) Microarray analyses of Srebp-1a and Srebp-1c target genes identify new regulatory pathways in muscle. *Physiol. Genomics* **34,** 327–337
43. Nakagawa, Y., Shimano, H., Yoshikawa, T., Ide, T., Tamura, M., Furusawa, M., Yamamoto, T., Inoue, N., Matsuzaka, T., Takahashi, A., Hasty, A. H., Suzuki, H., Sone, H., Toyoshima, H., Yahagi, N., and Yamada, N. (2006) TFE3 transcriptionally activates hepatic IRS-2, participates in insulin signaling, and ameliorates diabetes. *Nat. Med.* **12,** 107–113
44. Griffin, M. J., and Sul, H. S. (2004) Insulin regulation of fatty acid synthase gene transcription: roles of USF and Srebp-1c. *IUBMB Life* **56,** 595–600
45. Csernus, K., Lanyi, E., Erhardt, E., and Molnar, D. (2005) Effect of childhood obesity and obesity-related cardiovascular risk factors on glomerular and tubular protein excretion. *Eur. J. Pediatr.* **164,** 44–49
46. Porstmann, T., Santos, C. R., Griffiths, B., Cully, M., Wu, M., Leevers, S., Griffiths, J. R., Chung, Y. L., and Schulze, A. (2008) Srebp activity is regulated by mTORC1 and contributes to Akt-dependent cell growth. *Cell Metab.* **8,** 224–236
47. Betz, C., and Hall, M. N. (2013) Where is mTOR and what is it doing there? *J. Cell Biol.* **203,** 563–574
48. Satriano, J., and Sharma, K. (2013) Autophagy and metabolic changes in obesity-related chronic kidney disease. *Nephrol. Dial. Transplant.* **28,** Suppl. 4, iv29–36
49. Yasuda, M., Tanaka, Y., Kume, S., Morita, Y., Chin-Kanasaki, M., Araki, H., Isshiki, K., Araki, S., Koya, D., Haneda, M., Kashiwagi, A., Maegawa, H., and Uzu, T. (2014) Fatty acids are novel nutrient factors to regulate mTORC1 lysosomal localization and apoptosis in podocytes. *Biochim. Biophys. Acta* **1842,** 1097–1108
50. Yamahara, K., Kume, S., Koya, D., Tanaka, Y., Morita, Y., Chin-Kanasaki, M., Araki, H., Isshiki, K., Araki, S., Haneda, M., Matsusaka, T., Kashiwagi, A., Maegawa, H., and Uzu, T. (2013) Obesity-mediated autophagy insufficiency exacerbates proteinuria-induced tubulointerstitial lesions. *J. Am. Soc. Nephrol.* **24,** 1769–1781
51. Thomas, M. E., and Schreiner, G. F. (1993) Contribution of proteinuria to progressive renal injury: consequences of tubular uptake of fatty acid bearing albumin. *Am. J. Nephrol.* **13,** 385–398
52. Liu, B., Chen, Y., and St Clair, D. K. (2008) ROS and p53: a versatile partnership. *Free Radic. Biol. Med.* **44,** 1529–1535
53. Johnson, T. M., Yu, Z. X., Ferrans, V. J., Lowenstein, R. A., and Finkel, T. (1996) Reactive oxygen species are downstream mediators of p53-dependent apoptosis. *Proc. Natl. Acad. Sci. U.S.A.* **93,** 11848–11852
54. Furukawa, S., Fujita, T., Shimabukuro, M., Iwaki, M., Yamada, Y., Nakajima, Y., Nakayama, O., Makishima, M., Matsuda, M., and Shimomura, I. (2004) Increased oxidative stress in obesity and its impact on metabolic syndrome. *J. Clin. Invest.* **114,** 1752–1761
55. Carmiel-Haggai, M., Cederbaum, A. I., and Nieto, N. (2005) A high-fat diet leads to the progression of non-alcoholic fatty liver disease in obese rats. *FASEB J.* **19,** 136–138
56. Jain, S. S., Paglialunga, S., Vigna, C., Ludzki, A., Herbst, E. A., Lally, J. S., Schrauwen, P., Hoeks, J., Tupling, A. R., Bonen, A., and Holloway, G. P. (2014) High-fat diet-induced mitochondrial biogenesis is regulated by mitochondrial-derived reactive oxygen species activation of CaMKII. *Diabetes* **63,** 1907–1913
57. Youn, J. Y., Siu, K. L., Lob, H. E., Itani, H., Harrison, D. G., and Cai, H. (2014) Role of vascular oxidative stress in obesity and metabolic syndrome. *Diabetes* **63,** 2344–2355